Monitoring biochemical limitations to photosynthesis in N and P-limited radiata pine using plant functional traits quantified from hyperspectral imagery

Michael S. Watt[1*], Henning Buddenbaum[2], Ellen Mae C. Leonardo[3], Honey Jane Estarija[3], Horacio E. Bown[4], Mireia Gomez-Gallego[5], Robin Hartley[3], Grant D. Pearse[3], Peter Massam[3], Liam Wright[3], Pablo J. Zarco-Tejada[6,7]

[1]Scion, 10 Kyle St, Christchurch 8011, New Zealand

[2]Environmental Remote Sensing and Geoinformatics, Trier University, 54286 Trier, Germany

[3]Scion, PO Box 3020, Rotorua, New Zealand

[4]Faculty of Forestry, Universidad de Chile, Casilla 9206, Santiago, Chile

[5]Department of Forest Mycology and Plant Pathology, Swedish University of Agricultural Sciences, Box 7026, 750 07 Uppsala, Sweden

[6]The University of Melbourne, Melbourne, Victoria 3010, Australia

[7]Instituto de Agricultura Sostenible (IAS), Consejo Superior de Investigaciones Científicas (CSIC), Alameda del Obispo s/n, 14004 Cordoba, Spain.

*Corresponding author: Tel: +64 7 343 5665; Email: michael.watt@scionresearch.com

Target Journal: Remote Sensing of Environment

Abstract

The prediction of carbon uptake by forests across fertility gradients requires accurate characterisation of how biochemical limitations to photosynthesis respond to variation in key elements such as Nitrogen (N) and Phosphorus (P). Over the last decade, proxies for chlorophyll and photosynthetic activity have been extracted from hyperspectral imagery and used to predict important photosynthetic variables such as the maximal rate of carboxylation (V_{cmax}) and electron transport (J_{max}). However, little research has investigated the generality of these relationships within the Nitrogen (N) and Phosphorus (P) limiting phases, which are characterised by mass based foliage ratios of N/P $\leq$ 10 for N limitations and N:P > 10 for P limitations.

Using measurements obtained from one year old *Pinus radiata* D. Don grown under a factorial range of N and P treatments this research examined relationships between photosynthetic capacity (V_{cmax}, J_{max}) and measured N, P and chlorophyll (Chl_{a+b}). Using functional traits quantified from hyperspectral imagery we then examined the strength and generality of relationships between photosynthetic variables and Photochemical Reflectance Index (PRI), Sun-Induced Chlorophyll Fluorescence (SIF) and chlorophyll *a*+*b* derived by radiative transfer model inversion.

There were significant (P<0.001) and strong relationships between photosynthetic variables and both N (R^2 = 0.82 for V_{cmax}; R^2 = 0.87 for J_{max}) and Chl_{a+b} (R^2 = 0.85 for V_{cmax}; R^2 = 0.86 for J_{max}) within the N limiting phase that were weak (R^2 < 0.02) and insignificant within the P limiting phase. Similarly, there were significant (P<0.05) positive relationships between P and photosynthetic variables (R^2 = 0.50 for V_{cmax}; R^2 = 0.58 for J_{max}) within the P limiting phase that were insignificant and weak (R^2 < 0.33) within the N limiting phase.

Predictions of photosynthetic variables using Chl_{a+b} estimated by model inversion were significant (P<0.001), positive and strong (R^2 = 0.64 for V_{cmax}; R^2 = 0.63 for J_{max}) within the N limiting phase but insignificant and weak (R^2 < 0.05) within the P limiting phase. In contrast,

both SIF and PRI exhibited moderate to strong positive correlations with photosynthetic variables within both the N and P limiting phases. These results suggest that quantified SIF and PRI from hyperspectral images may have greater generality in predicting biochemical limitations to photosynthesis than proxies for N and chlorophyll *a*+*b*, particularly under high foliage N content, when P is limiting.

Keywords: high resolution hyperspectral; J_{max}, leaf maximum carboxylation rate; N:P ratio; nutrient limitation; physically based models; radiative transfer; reflectance; V_{cmax}

1.Introduction

The use of optical data to predict biochemical, structural and physiological traits from leaves and plant canopies has increased rapidly over the last two decades (for reviews see Hill et al. 2019; Watt et al. 2019). Key attributes of interest that have been successfully estimated include water content (Buddenbaum et al. 2011; Buddenbaum et al. 2015; Colombo et al. 2008; Fang et al. 2017; Malenovský et al. 2006; Riaño et al. 2005), leaf morphological traits such as specific leaf area (Asner and Martin 2008) and leaf mass per area (Asner et al. 2011b; Doughty et al. 2011), pigments such as chlorophyll (Croft et al. 2014; Curran et al. 2001; Gitelson et al. 1996; Tsay et al. 1982; Yoder and Pettigrew-Crosby 1995; Zarco-Tejada et al. 2019), carotenoids (Hernández-Clemente et al. 2012; Hernández-Clemente et al. 2014) and foliar concentrations of most key nutrients, particularly nitrogen (N) and phosphorus (P) (Asner and Martin 2008; Asner et al. 2011a; Curran et al. 2001; Dechant et al. 2017; Gillon et al. 1999; Luther and Carroll 1999; Masaitis et al. 2014; Petisco et al. 2005; Schlerf et al. 2010; Serbin et al. 2014; Stein et al. 2014; Tsay et al. 1982; Wang et al. 2018; Wang et al. 2015; Yoder and Pettigrew-Crosby 1995). However, the remote sensing of attributes associated with photosynthesis has progressed at a far slower rate.

The rate of carbon assimilation under ambient conditions (A) is strongly influenced by light intensity, air temperature, water availability and leaf biochemistry (Farquhar et al. 1980; Leuning 1995). These factors have been combined into a C_3 photosynthesis model that shows the rate of carbon assimilation to be limited under ambient conditions by the maximal rate of ribulose-1,5-bisphosphate (RuBP) carboxylase-oxygenase (Rubisco) carboxylation (V_{cmax}) and the maximal electron transport rate driving regeneration of RuBP (J_{max}). In combination V_{cmax} and J_{max} define the plants biochemical limitations to photosynthesis and these two variables will be, hereafter, collectively termed photosynthetic capacity.

Previous research shows that photosynthetic capacity ranges widely both within and among species, and is sensitive to variation in environmental conditions (Groenendijk et al. 2011; Xu and Baldocchi 2003). Despite this variation, a fixed value for V_{cmax} is often assumed in Terrestrial Biosphere Models which provide the main means of predicting regional and global estimates of terrestrial carbon (Beer et al. 2010). Many studies have investigated the use of plant functional traits such as leaf phosphorus (P), specific leaf area (SLA) and leaf nitrogen (N) to account for variation in photosynthetic capacity (Walker et al. 2014). As N is a primary component of Rubisco and the light-harvesting complexes that regulate photosynthesis (Niinemets and Tenhunen 1997), studies have often successfully used N to predict photosynthetic capacity (Dechant et al. 2017), although seasonal variation in partitioning of N to photosynthetic fractions can complicate predictions (Croft et al. 2017). Chlorophyll content has also been found to be a useful predictor of photosynthetic capacity (Croft et al. 2017) as this pigment is involved in light harvesting and there is a direct relationship between this pigment and J_{max} (Collatz et al. 1991; Sellers et al. 1992), which in turn is usually strongly and linearly related to V_{cmax}, across a large range of species (Medlyn et al. 2002).

Chlorophyll fluorescence has been widely shown to serve as a proxy for electron transport rate and photosynthetic activity (Genty et al. 1989; Weis and Berry 1987). As chlorophyll fluorescence is dependent on chlorophyll concentration, which has been found to be closely aligned to photosynthetic capacity (Croft et al. 2017; Houborg et al. 2013), a strong link has also been shown between Sun Induced Chlorophyll Fluorescence (SIF) and V_{cmax} (Rascher et al. 2015). A recent review has outlined the progress in SIF retrievals over the last 50 years (Mohammed et al. 2019) and research has demonstrated the utility of SIF in predicting photosynthetic activity at both the leaf and the canopy scales from a range of remote sensing platforms (Cendrero-Mateo et al. 2015; Zarco-Tejada et al. 2013a; Zarco-Tejada et al. 2016).

A parallel line of investigation over the last two decades has focussed on the use of Photochemical Reflectance Index (PRI) to predict photosynthetic activity of vegetation. This

index, which is determined from narrow band reflectance at 531 and 570 nm (Gamon et al. 1992; Gamon et al. 1997) and in closely related bands in derivative versions (Gamon et al. 1993), has been widely used to predict photosynthetic status across a range of vegetation types. PRI provides a linkage with the efficiency of photosystem II through characterising variation in xanthophyll pigments and as such quantifies changes in non-photochemical quenching and light use efficiency (Gamon et al. 1997). This index has been successfully used to predict photosynthetic rate (Drolet et al. 2008; Fuentes et al. 2006; Gamon et al. 1997; Guo and Trotter 2004; Hilker et al. 2008; Middleton et al. 2009; Nichol et al. 2000; Penuelas et al. 1995; Stylinski et al. 2000) and the photosynthetic response of plants subject to a range of stresses (Dobrowski et al. 2005; Hernández-Clemente et al. 2011; Scholten et al. 2019; Suárez et al. 2008) and is responsive to seasonal changes in pigments (Gitelson et al. 2017). PRI can be readily used to scale photosynthesis to the canopy level as recently launched satellite based hyperspectral imagers (e.g. PRISMA, DESIS) and planned missions (e.g. EnMAP) are capable of measuring this variable. In addition, Sentinel-2 and in particular the Sentinel-3 satellite OLCI and SLSTR sensors enable the estimation of vegetation pigments using the red edge spectral region and spectral bands centered at the green region for the assessment of the xanthophyll pigment dynamics and V_{cmax} at global scales using the SCOPE model (Prikaziuk and van der Tol 2019). Although many studies show that PRI is an effective proxy for photosynthesis (Hernández-Clemente et al. 2019) the index has been shown to be affected by canopy structure, leaf pigments and background (Suárez et al. 2009; Suárez et al. 2008), which can negatively impact predictions of photosynthesis (Rascher and Pieruschka 2008).

In this context, physically based modelling has been widely used as a method for generalising the spatial prediction of important vegetation traits. As these models are able to account for the influence of variations in background, canopy architecture and conditions during the image acquisition on reflectance they can be more generally applied than other approaches (Hill et al. 2019; Watt et al. 2019). One of the most widely used models is PROSAIL which

uses PROSPECT (Jacquemoud and Baret 1990) to simulate leaf reflectance and transmittance which are then fed into SAIL (Verhoef 1984), which predicts canopy reflectance from this input and soil optical properties and illumination geometry (Berger et al. 2018). When PROSAIL is run in inverse mode this model can be used to predict chlorophyll content and other biochemical constituents of foliage from canopy reflectance (Le Maire et al. 2008; Zarco-Tejada et al. 2004b; Zhang et al. 2005). Given the importance of chlorophyll in the photosynthetic process, predictions of this pigment from PROSAIL have considerable potential for spatially describing variation in key photosynthetic variables. As described in the review by Jacquemoud et al. (2009) PROSAIL has been developed for homogeneous and uniform canopies, and requires more complex approximations to account for forest architecture. For this purpose, radiative transfer approaches such as DART (Gastellu-Etchegorry et al. 1996), 4-Scale (Chen et al. 1997) and FLIGHT (North 1996) have been used with success but these require a large number of inputs.

Considerable research has demonstrated that N and P independently limit both plant growth and photosynthetic capacity and that the N/P ratio can be used to partition ranges that are either limited by N or P (Bown et al. 2007; Domingues et al. 2010; Ingestad 1971, 1979; Ingestad and Lund 1986). The underlying premise of this approach is that a N/P ratio of 10 (Knecht and Göransonn 2004) marks a threshold and deviations from this lead to nitrogen (N/P $\leq$ 10) or phosphorus (N/P > 10) deficiencies (Aerts and Chapin 2000; Marschner 1995; Reich and Schoettle 1988). This assumption of independent limitations clearly influences how models linking photosynthetic capacity to predictors derived from hyperspectral data are interpreted. These hyperspectral predictors may have a stronger association with photosynthetic capacity within either the N or P limiting range or alternatively could be applied using a single equation across both ranges. Despite this, we are unaware of any research that has examined how generalisable relationships between key hyperspectral variables and photosynthetic capacity are within N and P limiting ranges.

Within the southern hemisphere *Pinus radiata* D. Don (radiata pine) is the most widely planted plantation species and is particularly abundant within New Zealand where it constitutes 90% of the 1.7 M ha plantation area (NZFOA 2018). A key limitation of photosynthesis and growth in *P. radiata* plantations is nutrient supply (Raison and Myers 1992; Sheriff et al. 1986; Watt et al. 2005) and previous research has established relationships between V_{cmax}, J_{max} and foliar concentration of N and P in this species (Bown et al. 2007; Walcroft et al. 1997). However, we are unaware of any research that has investigated the utility of hyperspectral imagery for predicting photosynthetic capacity in *P. radiata*.

In this study, measurements of hyperspectral imagery, foliage nutrition and photosynthesis were taken from an experiment that included a factorial combination of N and P treatments applied to *P. radiata*. Using this data, the overall goal of this research was to better understand the key determinants of photosynthetic capacity and how hyperspectral imagery can best be used to predict photosynthetic capacity. Specifically, we examined relationships between photosynthetic capacity and measured chlorophyll (Chl_{a+b}), N and P within both the N and P limiting ranges. Using plant functional traits derived from hyperspectral data we then explored the strength and generality of relationships between photosynthetic capacity and PRI, SIF and chlorophyll *a+b* derived by radiative transfer model inversion.

2. Methods

2.1. Experimental set up

The experiment was undertaken within the Scion nursery, located in Rotorua, New Zealand. A total of 120 *P. radiata* seedlings were transplanted into pots with a 15 L volume during October 2018. The medium into which the plants were transplanted consisted of a mixture of perlite and vermiculite which are silica-based products without any nutritional content. Plants were grown

in a thermostatically controlled greenhouse where temperature in spring fluctuated between 10 and 24 °C during the day and between 10 and 16 °C during the night. These plants were watered weekly over the duration of the trial so that root-zone water content did not limit growth. This study reports on detailed measurements taken from a subsample of 30 trees, within this trial, that included six trees from each of the five treatments.

The five fertiliser treatments consisted of a factorial combination of N and P that were applied as 500 ml of nutrient solution per plant every fortnight starting on the 20th February, 2019. These five treatments included application of water only (Control), low N–low P (N0P0), low N–high P (N0P1), high N–low P (N1P0) and high N–high P (N1P1). Nutrient solutions consisted of two levels of nitrogen (N0 = 1.43 and N1 = 7.14 mol m^{-3}) and phosphorus (P0 = 0.084 and P1 = 0.420 mol m^{-3}). Following Ingestad (1979) N was provided at concentrations of 100 ppm (7.14 mM) and P at 13 ppm (0.420 mM) as the high-N and high-P supply regimes. The low-N (1.43 mM) and low-P (0.084 mM) supply regimes were chosen as one-fifth of the high-N and high-P concentrations, respectively. Nitrogen was supplied as NH_4NO_3 and phosphorus as KH_2PO_4 and nutrients other than N and P were provided in optimum proportions in relation to N, as defined by Ingestad (Ingestad 1971, 1979).

2.2. Hyperspectral data capture

2.2.1 Data capture

A hyperspectral camera (FX10, Specim, Spectral Imaging Ltd, Oulu, Finland) was used to acquire hyperspectral imagery outside of the greenhouse, under clear sky conditions, from 10:30 am to 1:30 pm on the 4th October, 2019. This push-broom camera captures 448 bands with wavelengths ranging from 400 to 1000 nm with a spectral full width at half maximum (FWHM) of 5.5 nm. The camera is designed for industrial applications and as such has a high maximum

frame rate of 9900 frames per second with one band, and 330 frames per second using the full range of bands, as well as a high Signal-to-Noise Ratio (SNR) of 600:1. Within the field of view of 38° the spatial sampling comprises 1024 pixels. We used the Lumo Recorder software interface to manage the image acquisition.

The camera was mounted 2 m above ground on a cross beam that was supported by two posts, and a conveyor belt was used to move the plants through the field of view. The speed of the conveyor belt was adapted to fit the frame rate of the camera, which in turn was dependent on the exposure time, which had to be adjusted to the current illumination conditions. During the measurements, the conveyor belt speed and frame rate were kept constant and the exposure time was adjusted to avoid over or undersaturation. A diffuse white reference standard (Spectralon, North Hutton, NH, USA) was placed so that it was visible in every frame allowing calibration of the imagery as a function of the changing illumination conditions.

2.2.2. Pre-processing of hyperspectral data

All pre-processing of the hyperspectral data was carried out using Matlab (The MathWorks, Inc., Natick, Massachusetts, United States) following the methods described in Buddenbaum et al. (2019). Pixels with NDVI ≥ 0.5 and reflectance at 780 nm ≥ 0.2 were selected as vegetation pixels. Pixels with absolute first difference values ≥ 0.1 were masked out. Sample reflectance spectra for trees that are representative of the treatments are shown in Figure 1. Following these steps the number of pixels selected ranged from 16,000 – 112,000 pixels/tree, with an average of 52,267 pixels/tree. The mean of all pixels for each tree was calculated to represent the whole plant.

Following these steps, the tree level spectra were smoothed using the Savitzky-Golay filter (Mouazen et al. 2010) as this filter has consistently been found to be one of the best available pre-

processing transformations (Vasques et al. 2008). This smoothing used a third order polynomial which was applied across a moving window of 27 spectral bands. Reflectance and the 1st derivative of reflectance were extracted from these smoothed spectra. As there was considerable noise at either end of the smoothed spectral data, the 52 bands that occurred both below 415 nm and above 951 nm, were excluded from further analyses. Following these exclusions, 396 bands (415 – 951 nm) describing reflectance and 395 bands (416 – 951 nm) describing the 1st derivative of reflectance were available for analyses.

2.2.3. Radiative transfer model inversion

Pure vegetation reflectance spectra extracted from the hyperspectral data acquired from the seedlings was used to invert PROSAIL to estimate chlorophyll *a*+*b* content ($Chl_{a+b\ PROSAIL}$). Although SAIL is designed for homogeneous canopies and this condition was not met by our experimental set-up, an inversion of PROSAIL was undertaken (Jacquemoud et al. 2009) using the spectra extracted from pure vegetation pixels (as in Zarco-Tejada et al. 2018). The PROSPECT model has been demonstrated to be valid for simulating needle reflectance in Jack Pine (*Pinus banksiana* Lamb.) stands for chlorophyll *a*+*b* content estimation (Zarco-Tejada et al. 2004a). The proposed PROSPECT and SAIL models used here were successful for chlorophyll content estimation when targeting pure vegetation pixels in forest areas (Zarco-Tejada et al. 2001). Thus, we used a combination of PROSPECT-D (Féret et al. 2017) and 4SAIL (Verhoef et al. 2007) model versions, and inverted the spectra using the function lsqcurvefit in Matlab, following an approach by Jay et al. (2016). Parameters with low sensitivity were fixed so that only a limited number of parameters needed to be optimized. The leaf inclination distribution type was set to 2 so that only the average leaf inclination angle (ALA) was included in the model. The soil spectrum was also fixed. The model code includes spectra for a dark wet and a bright

dry soil. We used a linear combination of 10% dark soil and 90% bright soil. Further model parameters are listed in Table 1.

2.2.4. Calculation of PRI and Sun Induced Chlorophyll Fluorescence quantification

The reflectance spectra were interpolated to a 1 nm resolution within Matlab. Using the interpolated spectra, calculations of PRI ($PRI_{531,570}$) were made using the following (Gamon et al. 1992),

$$PRI = (R_{531} - R_{570})/ (R_{531} + R_{570}) \quad (1)$$

We also trialled an alternative formulation of PRI ($PRI_{528,567}$) that utilised 528 nm and 567 nm (Gamon et al. 1993) and this variation was used in analyses as it was more precisely correlated to photosynthetic capacity than $PRI_{531,570}$. Although PRI was developed to track changes in xanthophyll pigments, it has been reported that such spectral bands in the 530-570 nm region are also influenced by confounding effects related to the absorption of other photosynthetic pigments, structure of the canopy, and the soil and background (Suárez et al. 2009; Suárez et al. 2008; Zarco-Tejada et al. 2013b). Thus, changes observed in PRI are potentially due to the combined changes of chlorophyll and xanthophylls, and structural effects over the course of the experiment.

Sun-Induced Chlorophyll Fluorescence (SIF) was quantified using the 760 nm O_2-A band using the *in-filling* method based on the Fraunhofer Line Depth principle (FLD) calculated from a total of three spectral bands (FLD3) as follows,

$$SIF = \frac{E_{out}\, L_{in} - E_{in}\, L_{out}}{E_{out}\, E_{in}} \quad (2)$$

where radiance, L, corresponds to L_{in} (L_{761}), L_{out} (average of L_{747} and L_{780} bands), and the irradiance, E, to E_{in} (E_{761}), and E_{out} (average of E_{747} and E_{780} bands). Values of SIF were rescaled through addition of an offset value to ensure that calculations of SIF from Equation 2 were not negative.

2.3. Photosynthetic capacity

Measurements of photosynthetic capacity were made using a coupled chlorophyll fluorescence and gas-exchange system (Imaging-PAM M-Series and GFS-3000, Walz, Effeltrich, Germany) from the 7th to 16th of October 2019 following measurements of hyperspectral data. For each of the 30 plants, the response of assimilation to intercellular CO_2 concentration (A/C_i response) was measured on two to three fully expanded young fascicles that were selected from the upper third of the canopy. These needles were arranged inside the 6 cm^2 cuvette without overlap and the area for these needles was determined by differentiating thresholded pixels using the Imaging-Win software of the coupled system. During the course of the measurements, conditions in the cuvette were maintained at 20 °C, with a relative humidity of 60% and an irradiance of 1,000 μmol photons m^{-2} s^{-1}. The external CO_2 concentration (C_a) supplied to the plants included the following series: 400, 300, 200, 100, 75, 50, 400, 600, 800, 1000, 1200, 1500, 2000 μmol mol^{-1}. Measurements were recorded after values of A, C_i and g_s were stable.

A/C_i curves were analysed using Farquhar-type equations (Long and Bernacchi 2003). A generalised nonlinear least squares regression (*gnls* function, nlme package in R) was used to estimate V_{cmax} and J_{max}.

2.4. Determination of foliage N, P and Chlorophyll

315 Following the completion of the A/C_i response curves, approximately 10 fully extended fascicles,
316 were selected from the upper third of the crown of each plant. These fascicles were dried at 70°
317 C for at least 48 hours to constant dry mass and transported to the Landcare Research laboratory
318 (Palmerston North, New Zealand) for analysis of N and P. Foliage samples were finely ground,
319 acid digested by the Kjeldahl method, and the N and P concentrations were determined
320 colorimetrically (Blakemore et al. 1987). Approximately 20 fully extended fascicles were
321 selected for measurements of chlorophyll *a*+*b* (Chl_{a+b}). These needles were placed in tubes and
322 frozen at -80ºC before being transported with dry ice to Plant and Food Laboratory (Lincoln, New
323 Zealand) where analysis was undertaken using Chl_{a+b} estimation by spectrometry. From finely
324 ground foliage samples, plant materials were extracted with acetone. This extraction was
325 undertaken in the dark and the samples were kept on ice throughout the process to avoid pigment
326 degradation. The absorbance of the extracts in the wavelengths 645, 652, 663, and 700 nm were
327 read against 80% acetone and these values were then used to compute the chlorophyll
328 concentration (Holden 1965). All values of chlorophyll reported here refer to the total chlorophyll
329 (Chl_{a+b}).

330 Specific leaf area, (SLA) was determined from needles sampled for chlorophyll and
331 expressed on a hemi-surface leaf area basis. Following Bown et al (2009b) leaf area was
332 determined from $[nld(1 + \pi/n)]/2$, where *d* is fascicle diameter, *l* is fascicle length and *n* is the
333 number of needles per fascicle. SLA was expressed in μg cm^{-2} as the quotient of dry weight and
334 leaf area. Measurements of SLA were used to convert foliage nutrient and pigment concentrations
335 to a hemi-surface area basis.

336

337 *2.5. Measurements of tree dimensions*

338

339 Tree height, root collar diameter and crown diameter were measured on the 22nd of October.
340 Crown diameter was measured in two perpendicular directions at the widest point and these

measurements were averaged. Electronic calipers were used to measure root collar diameter and both height and crown width were measured using a tape.

2.6. Data analysis

All analyses were undertaken at the plant level using a combination of Matlab (The MathWorks, Inc., Natick, Massachusetts, United States) and R (R Development Core Team 2011). Matlab was used to plot the spectra and invert PROSAIL while all other analyses were undertaken using R.

2.6.1. Treatment differences

Tree dimensions, foliage nutrient content, photosynthetic variables, and PROSAIL output were tabulated and one-way analysis of variance was used to test for treatment differences between these variables. Multiple range testing, using the Tukey test, was used to determine which treatments significantly differed for all variables in which treatment had a significant effect.

Treatment variation in hyperspectral variables was plotted. We undertook a one-way analysis of variance across each of the 396 reflectance bands to identify which bands were most sensitive to the treatments. This band level ANOVA was also undertaken on four different treatment contrasts to isolate the influence of N and P on reflectance. The influence of N was determined through contrasting reflectance for low and high N treatments at both low (N0P0 vs N1P0) and high P (N0P1 vs. N1P1). Similarly, the influence of P on reflectance was identified through contrasting low and high P treatments at both low (N0P0 vs N0P1) and high N (N1P0 vs. N1P1). Using a Bonferroni correction these contrasts were deemed to be significant at $P < 0.0125$.

2.6.2 Prediction of photosynthetic variables

Nutrient ratios were used to separate the dataset into plants that were either N or P limiting to gain greater insight into the processes regulating photosynthetic capacity within each of these two phases. Following previous literature (Aerts and Chapin 2000; Knecht and Göransonn 2004; Marschner 1995; Reich and Schoettle 1988) trees with an N/P ratio (expressed on a mass basis) of ≤ 10 were categorised as N deficient, while those with N/P > 10 were categorised as P deficient. The foliage N/P within sampled trees ranged from 2.6 – 27.9, of which 9 observations were P limited while the remaining 21 were N limited (Fig. 2).

Following Kattenborn et al. (2019) all modelling used nutrient concentrations expressed on an area basis. Initial analyses examined correlations between N, P, and PRI and SIF. Bivariate relationships were then developed between the photosynthetic variables and N, P, Chl_{a+b} to examine the role that these variables played in regulating photosynthetic capacity. The potential of predicting V_{cmax} and J_{max} from hyperspectral data was then investigated through development of models that included either $Chl_{a+b\ PROSAIL}$, PRI or SIF. In all developed models only significant variables were included in the models and variables were used in the models in either linear formulations, and where significant, in a polynomial formulation.

3. Results

3.1. Tree characteristics

All physical dimensions varied significantly between treatments (Appendix 1) and dimensions for the two high N treatments were markedly greater than those for the three low N treatments. Mean height, root collar diameter and crown width in N1P1 were, respectively, 85.8 cm, 15.9 mm and 31.6 cm, which exceeded corresponding mean values for these three dimensions in the Control, N0P1 and N0P1, by respectively, 58, 31 and 64%. There were no significant treatment differences in SLA and values averaged 2,467 µg cm^{-2} across treatments (Appendix 1).

393

394 *3.2 Foliar nutrition*

395

396 The applied treatments resulted in a wide range in N and P (Fig. 2) and both elements significantly
397 varied between treatments when expressed on either a mass or area basis (Appendix 1). Values of
398 N ranged from 0.41 – 2.00 % when expressed on a mass basis and 11.1 – 45.8 µg cm^{-2} on an area
399 basis while P varied from respectively 0.053 – 0.278 % and 1.41 – 6.47 µg cm^{-2}. The relationship
400 between N and P was weakly significant (Fig. 2) when data was expressed on a mass basis (P =
401 0.03; R^2 = 0.224) but insignificant when expressed on an area basis (P = 0.10; R^2 = 0.155). The
402 relationship between N and Chl_{a+b} was positive, highly significant and very strong when expressed
403 on either a mass (P <0.001; R^2 = 0.887) or area basis (P <0.001; R^2 = 0.870).
404 When expressed on an area basis there were no significant differences in N or Chl_{a+b}
405 (Appendix 1) between the two high N treatments (N1P0, N1P1) or the two low N treatments
406 (N0P0, N0P1). Similarly, P did not significantly differ between the two low P treatments (N0P0,
407 N1P0) or the two high P treatments (N0P1, N1P1). There was an identical significance pattern
408 for N, P and Chl_{a+b} expressed on a mass basis (Appendix 1), except for the pairwise comparison
409 of N for the two high N treatments (N1P0 and N1P1) which exhibited significant differences.
410 This low level of lack of significance provided a sound basis for the pairwise testing of the
411 impacts of N and P on both photosynthetic capacity and hyperspectral imagery, that is described
412 below.

413

414 *3.3. Photosynthesis capacity*

415

416 Differences between treatments were highly significant for both V_{cmax} and J_{max} (P<0.001). The
417 mean values of V_{cmax} and J_{max} for N1P1, were respectively, 34.9 and 90.5 µmol m^{-2} s^{-1} which
418 exceeded those in the Control treatment by ca. three-fold for both variables (Appendix 1). Most

variation between the treatments was attributable to addition of N (Appendix 1). Values for the two high N treatments (N1P0, N1P1) significantly exceeded those of the two low N treatments, with equivalent P additions (N0P0, N0P1) by respectively 55 and 51% for V_{cmax} and J_{max} (Appendix 1). Addition of P to the low N treatment (i.e. N0P1 vs N0P0) increased V_{cmax} and J_{max} by respectively 7.8 and 3.3%, while addition of P to the high N treatment (i.e. N1P1 vs N1P0) resulted in greater increases to V_{cmax} and J_{max} of respectively, 11.5 and 16.2% (Appendix 1).

3.4. Hyperspectral data

Figure 3 shows variation in canopy reflectance and the 1st derivative of reflectance at the tree level while Figure 4 describes variation in reflectance across the entire spectrum and within three narrow wavelength ranges for data averaged by treatment (Fig. 4 a – d) and type of limitation (Fig 4e – h). Tree level variation in reflectance was relatively tightly clustered within treatments highlighting the consistency of the data (Fig. 3a). Treatment level reflectance was higher in the low N treatments between 450 – 680 nm with the highest values recorded in the Control treatment (4a – d). There was also a marked shift in the lower wavelengths of the red edge for the low N treatments compared to those with high N (Fig. 4d). Both of these treatment influences on reflectance were significant, with the highest levels of significance occurring at wavelengths centred in the red edge at 700 nm and the green peak at 580 nm (Fig. 5), with significant treatment differences occurring at all other wavelengths between 472 – 728 nm (Fig. 5).

The first derivative of reflectance for the three low N treatments exhibited marked increases between 500 – 550 nm (Fig. 3b), compared to the two high N treatments and peak values for the first derivative were reached at lower wavelengths, with both features being most marked for the Control treatment (Fig. 3b). Significant treatment differences were noted in the

first derivative in almost all wavelengths between 422 – 811 nm with the most significant differences occurring at wavelengths centred around 497 and 647 nm (Fig. 5).

Analysis of variance, using treatment combinations that partitioned the impact of N and P, showed that treatment differences were mainly attributable to variation in N. For reflectance, comparisons of low and high P at similar values of N, that were either low (i.e. N0P0 vs. N0P1, red circles, Fig. 6a) or high (i.e. N1P0 vs. N1P1, blue circles, Fig. 6a) did not significantly differ. The small influence of P on reflectance is also clearly evident in figures showing spectral changes across discrete ranges which shows these two P contrasts almost overlap between 400 – 700 nm (Figs. 4b – d). Similarly, for the first derivative, these two treatment comparisons were mostly non-significant, with the exception of a few wavelengths, scattered across the spectral range (Fig. 6b).

In contrast, comparisons of reflectance for low and high N, made at low values of P (green circles, Fig. 6a) or high values of P (black circles, Fig. 6a) showed significant differences between treatments from ca. 500 – 730 nm, reaching highest significance for both comparisons in the red edge region, and at wavelengths centred around 534 nm for N0P1 vs. N1P1 (Fig. 6a). Treatment contrasts shown for discrete spectral regions (Figs 4b – d) show that higher N markedly reduces reflectance, compared to low N, for both contrasts and that these differences are particularly marked within the green peak region (Fig. 4c).

Treatment comparisons were in general more significantly different for the first derivative of reflectance than reflectance (Fig. 6b). Differences in the first derivative for these two N treatment comparisons were significant across most of the spectral range, from ca. 432 – 763 nm, with the most significant values occurring in the red-edge region for N0P0 vs. N1P0 and at wavelengths centred around 504, 608 and 651 nm for N0P1 vs. N1P1 (Fig. 6b).

When expressed by the type of limitation, trees that were limited by N had higher reflectance than P limited trees within both the red edge range and visible spectrum above 430 nm (Fig. 4e). These differences were most marked within the green peak region (Fig. 4g). There

was also a marked shift in the lower wavelengths of the red edge for the N limited plants compared to those that were P limited (Fig. 4h).

3.5 Relationships between nutrient content and spectral indices

Within the N limiting range there were significant positive relationships between N and both PRI ($P < 0.001$; $R^2 = 0.83$; Fig 7a) and SIF ($P < 0.001$; $R^2 = 0.59$; Fig. 7c) but relationships between N and both of these variables were insignificant and weak, within the P limiting range (Fig. 7a, c). In the P limiting range, strong significant positive relationships were found between P and both SIF ($P < 0.01$; $R^2 = 0.697$) and $PRI_{528, 567}$ ($P < 0.001$; $R^2 = 0.792$), as shown by the filled blue circles, respectively, in Figures 7d and b. Within the N limiting range, the relationship between P and SIF was insignificant and weak ($P = 0.23$; $R^2 = 0.076$), while the relationship between P and $PRI_{528, 567}$ was only marginally significant but very weak ($P = 0.048$; $R^2 = 0.190$).

3.6 Models of photosynthetic capacity

3.6.1 Use of measured variables

Under both N and P limiting conditions Chl_{a+b} was most strongly related to both V_{cmax} ($P < 0.001$; $R^2 = 0.85$) and J_{max} ($P < 0.001$; $R^2 = 0.82$) and both relationships were positive (Fig. 8a, c; Table 2). There were strong positive relationships between N and both V_{cmax} ($P < 0.001$; $R^2 = 0.84$) and J_{max} ($P < 0.001$; $R^2 = 0.82$), that were only marginally weaker than the relationships with Chl_{a+b} (Fig. 9a, c; Table 2). Under N limiting conditions these relationships generally remained at similar strength, although N was a slightly stronger predictor of J_{max} than Chl_{a+b} ($R^2 = 0.87$ vs. 0.86). Under P limiting conditions, relationships between photosynthetic capacity and

either N (Fig. 9 a, c) or Chl $_{a+b}$ (Fig. 8 a, c) were very weak ($R^2 < 0.02$) and insignificant (Table 2).

Under P limiting conditions, relationships between P and both V_{cmax} (Fig 9b) and J_{max} (Fig 9d) were positive, significant and of a moderate strength, with respective R^2 of 0.50 and 0.58 (Table 2). In contrast, relationships between P and photosynthetic capacity (V_{cmax}, J_{max}) were insignificant under either N limiting conditions or across the entire dataset (Figs. 9b, d; Table 2).

3.6.2. Use of derived variables

There was a strong linear relationship ($R^2 = 0.88$) between area based measured chlorophyll (C_{a+b}) and chlorophyll predicted by model inversion ($C_{a+b\ PROSAIL}$). Values of C_{a+b} were overpredicted by $C_{a+b\ PROSAIL}$ at low values and underpredicted at high values, but there was little treatment bias in the predictions (Fig. 10).

Using all the data, $Chl_{a+b\ PROSAIL}$ exhibited strong positive linear relationships (Fig. 8b, d) with both V_{cmax} ($P < 0.001$; $R^2 = 0.79$) and J_{max} ($P < 0.001$; $R^2 = 0.76$). These relationships remained significant and relatively strong using data restricted to N limiting conditions (Table 2). However, there was no significant relationship between $Chl_{a+b\ PROSAIL}$ and either both V_{cmax} and J_{max} under P limiting conditions, with $R^2 < 0.04$ for both relationships (Table 2; Fig. 8b, d).

Using all the data there were strong relationships between $PRI_{528, 567}$ and both V_{cmax} ($P < 0.001$; $R^2 = 0.84$) and J_{max} ($P < 0.001$; $R^2 = 0.84$) that were best described using quadratic terms (Table 2; Fig. 11a, c). These relationships remained strong, but the precision was slightly reduced when data was restricted to N limiting conditions (Table 2). Under P limiting conditions positive correlations of moderate strength were found between $PRI_{528, 567}$ and V_{cmax} ($P = 0.06$; $R^2 = 0.42$) and J_{max} ($P = 0.029$; $R^2 = 0.51$), that were generally aligned with predictions under N limiting conditions (Table 2; Fig. 11a, c).

Using all the data SIF exhibited strong positive linear relationships with both V_{cmax} ($P < 0.001$; $R^2 = 0.78$) and J_{max} ($P < 0.001$; $R^2 = 0.80$), which were slightly reduced in strength when data was restricted to N limiting measurements (Table 2; Fig. 11b, d). Under P limiting conditions, SIF was moderately related to V_{cmax} ($P = 0.09$; $R^2 = 0.35$) and strongly related to J_{max} ($P < 0.01$; $R^2 = 0.68$) and these relationships aligned very well with predictions made under N limiting conditions (Fig. 11b, d).

Discussion

Our results show that N and P were only significantly related to V_{cmax} and J_{max}, within the N and P limiting ranges, respectively, suggesting that photosynthetic capacity is independently regulated by these elements. Predictions of photosynthetic capacity (V_{cmax}, J_{max}) using variables derived from hyperspectral imagery showed contrasting generality across the dataset. Strong positive relationships were observed between $Chl_{a+b\ PROSAIL}$ and both V_{cmax} and J_{max} in the N limiting phase but these relationships were insignificant in the P limiting range. However, both SIF and $PRI_{528, 567}$ exhibited moderate to strong positive relationships with photosynthetic capacity in both the N and P limiting phases suggesting that these variables are more generalisable than $Chl_{a+b\ PROSAIL}$.

The treatments used here created a wide range in N and P that exceeded the ranges in content and N/P ratio typically found in field grown *P. radiata*. When expressed on a mass basis foliage N ranged from 0.41 to 2.0% while foliage P ranged from 0.05 to 0.28%. Within a designed field experiment, located at 20 sites spanning almost all variation in soil fertility found in New Zealand plantations, ranges were markedly lower varying from 0.75 – 1.64% for N and from 0.09 – 0.18% for P (Watt et al. 2009). Our reported values in N and P covered ranges considered to be deficient, marginal and sufficient for both elements (Mead 2013).

The use of ratios provided a useful means of separating N from P limitations. Nutrient ratios have been extensively used to identify optimum nutrition and account for particular nutrient limitations (Ingestad 1971, 1979; Ingestad and Lund 1986). In terrestrial plants an optimum N/P ratio of 10 has been found for a wide range of species (Knecht and Göransonn 2004) which agrees with our results that show photosynthetic capacity peaks at ratios of 9.3 – 11.3 (data not shown). Several authors (Aerts and Chapin 2000; Marschner 1995; Reich and Schoettle 1988) suggest that deviations from this N/P ratio of 10 should lead to nitrogen (N/P ≤ 10) or phosphorus (N/P > 10) deficiencies. Our results strongly support this suggestion through showing that N and P were only significantly related to V_{cmax} and J_{max}, within the N and P limiting ranges, respectively.

Overall our results show that Chl_{a+b} and N had the largest influence on photosynthetic capacity. The strong relationships found here between photosynthetic capacity and both Chl_{a+b} and N under N limiting conditions have a sound physiological basis. Nitrogen is a major component of Rubisco (Niinemets and Tenhunen 1997) and at least 50% of leaf nitrogen is invested in the photosynthetic apparatus of plants (Niinemets and Sack 2006). As Rubisco catalyses the carboxylation reaction, there is a mechanistic link between the leaf Rubisco content and the maximum capacity of carboxylation, V_{cmax}.

Similarly, chlorophyll also plays an important role in photosynthesis. Chlorophyll which is embedded in the thykaloid membranes of chloroplasts, provides the principal means of harvesting light (Croft et al. 2017). This light harvest provides the energy to supply electrons, via the cytochrome b_6f complex, to produce nicotinamide adenine dinucleotide phosphate (NADPH) and chemical energy as adenosine triphosphate (ATP), for the reactions of the Calvin–Benson cycle. Chlorophyll content has been shown to be related to the amount of light harvested across a range of species (Collatz et al. 1991; Evans 1996), and photosynthetically active radiation absorbed by the leaf drives the potential rate of electron transport, J (Collatz et al. 1991; Sellers et al. 1992). Although Chl is theoretically more closely related to J_{max}, in

practice a strong linear relationship between V_{cmax} and J_{max}, is often observed across a range of species (Medlyn et al. 2002) as was found for our data (P <0.001; R^2 = 0.939). This tight coupling, which is thought to reflect coordination between these two rate- limiting biochemical cycles (Kattge and Knorr 2007; Leuning 1997; Medlyn et al. 2002; Walker et al. 2014), means that in practice Chl_{a+b} can be used as a predictor for both variables.

Under N limiting conditions, relationships between photosynthetic capacity and both Chl_{a+b} and N were found to have a very similar precision. This suggests that wavelengths associated with N in the SWIR range are not as important for predicting photosynthetic capacity in *P. radiata* as those associated with chlorophyll in the VNIR range. Examination of spectral differences between treatments confirm the importance of chlorophyll as a key predictor of photosynthetic capacity. These analyses show the most significant treatment differences occur within the green and red edge spectral regions which have previously been found to be key spectral predictors of chlorophyll content (Carter 1994; Gitelson and Merzlyak 1996; Horler et al. 1983; Rock et al. 1988; Vogelmann 1993).

The significant positive relationships that we found between P and both V_{cmax} and J_{max} within the P limiting range were associated with high values of N. Results from a *P. radiata* nutrition experiment with a similar design (Bown et al. 2009a), that investigated relationships between nutrition and photosynthetic capacity, were very similar to ours and found a significant relationship between P and photosynthetic capacity in the P limiting range. This result is also consistent with a meta-study undertaken by Walker (2014) who observed little gain in V_{cmax} and J_{max} under increasing P at low N, but a doubling of modelled gross carboxylation rates across a P range under high N levels, which is analogous to the P limiting range in our study. The importance of P in regulating V_{cmax} and J_{max} has a sound theoretical basis as the availability of P has an impact on many important aspects of photosynthesis including membrane solubility, ATP, and NADPH production (Marschner 1995; Taiz et al. 2015).

Our results demonstrate very little spectral alteration associated with P but do show significant relationships between P and both $PRI_{528, 567}$ and SIF within the P limiting range. After controlling for N, results clearly show little discernible change in reflectance or the first derivative of reflectance between plants with high or low P. This is consistent with previous literature as P does not directly absorb energy in the shortwave spectrum and consequently predictions of P typically rely on strong positive correlations with N (Asner and Martin 2008; Gillon et al. 1999; Porder et al. 2005). While this is a useful approach for vegetation with normal ratios of N and P, this empirical relationship is likely to break down when ratios of N and P deviate from normal values, and there is little correlation between N and P. Within the P limiting range there were moderate to strong positive, linear relationships between P and both SIF and PRI suggesting that these variables may act as proxies for P and the effect of this element on photosynthetic capacity.

Although the three variables, derived from the hyperspectral data, used to predict photosynthetic capacity had similar precision, there were marked differences in their utility for predicting photosynthetic capacity. The significant relationship found here between $Chl_{a+b\ PROSAIL}$ and photosynthetic capacity is consistent with previous research that has used chlorophyll derived from physically based models to predict V_{cmax} and J_{max} (Croft et al. 2017; Dechant et al. 2017). Our results generally support Croft et al (2017), who advocate the use of chlorophyll as a potentially useful proxy for photosynthetic capacity but extend these findings through showing that chlorophyll should be used with caution under P limiting conditions, where we found this relationship to be weak and insignificant.

SIF was strongly correlated with both V_{cmax} and J_{max} and, in contrast to $Chl_{a+b\ PROSAIL}$, predictions exhibited relatively robust correlations across both the N and P limiting ranges. Although SIF has been widely used to predict gross primary productivity (Meroni et al. 2009; Porcar-Castell et al. 2014; Rascher et al. 2015), and photosynthesis (Frankenberg et al. 2011; Guanter et al. 2014; Smith et al. 2018), in a range of species, with few exceptions (Camino et al.

2019) little research has linked SIF to V_{cmax} and J_{max} at a fine scale. As found here, there is generally a strong relationship between Chl and SIF as leaves with a higher Chl will absorb more light and produce a higher leaf SIF, although this effect is complicated by the fact that emitted SIF is scattered and reabsorbed throughout the canopy (Verrelst et al. 2015). It has been hypothesised that SIF is a useful predictor of photosynthetic capacity as it can be used to selectively measure the quantity of absorbed light in chlorophyll (Rascher et al. 2015). However, in contrast to Chl_{a+b}, our results suggest that SIF can at least partially account for the role of P on photosynthetic capacity at high values of N as supported by the strong relationship found between SIF and P under P limiting conditions.

Similarly, PRI was also strongly related to photosynthetic capacity and was able to account for variation in V_{cmax} and J_{max} across both N and P limitations. Research has widely demonstrated the utility of PRI for predicting light use efficiency (Garbulsky et al. 2011; Peñuelas et al. 2011) and key photosynthetic parameters under a range of stresses including severe drought conditions (Ripullone et al. 2011), cold winter temperatures (Gamon et al. 2016; Wong and Gamon 2015a, b) and herbicide damage (Scholten et al. 2019). The relationship found here between PRI and photosynthetic capacity is consistent with Scholten et al. (2019) and has a strong theoretical basis as PRI can track plant photosynthetic activity through its intimate link with the dissipation of excess energy by nonphotochemical quenching (NPQ) via the xanthophyll cycle. The xanthophyll cycle is activated during periods of excess excitation energy in the leaf and through this process violaxanthin is de-epoxidized to zeaxanthin. These increased concentrations in zeaxanthin reduce reflectance at wavelengths around 531 nm, which results in reductions in PRI. Nevertheless, PRI has been demonstrated to be related to the absorption of chlorophyll content, in addition to the xanthophyll pigments, as well as by the canopy structure and soil (Suárez et al. 2009; Suárez et al. 2008; Zarco-Tejada et al. 2013b). Results shown in this experiment show the potential contribution of both xanthophylls and chlorophyll in the observed relationships with photosynthetic capacity. As with SIF, our results

suggest that PRI may provide a more generalisable means of predicting photosynthetic capacity under a range of nutritional limitations than chlorophyll derived from physically based models.

Predictions of photosynthetic capacity estimated by PRI and SIF could be scaled up using satellite imagery. As summarised in Mohammed et al. (2019) measurements of SIF are currently taken from a number of satellite platforms (e.g. GOME-2, OCO-2) and the first satellite mission designed for SIF measurement, FLEX, is scheduled for launch in 2022. The recently launched PRISMA and DESIS hyperspectral imagers, and the EnMAP sensor, which is scheduled for launch in 2021, are particularly suitable for estimating PRI and will provide imagery at a spatial resolution of 30 m with a relatively fine spectral resolution of up to 6.5 nm within the VNIR range (Guanter et al. 2015). In addition, Sentinel-3 has been proposed for V_{cmax} estimation at global scales using radiative transfer models such as SCOPE (Prikaziuk and van der Tol 2019).

In conclusion, results from this study clearly demonstrate the utility of SIF and PRI for prediction of photosynthetic capacity across both the N and P limiting ranges. Although results clearly highlight the importance of N and Chl_{a+b} as key predictors of photosynthetic capacity we also show that these relationships break down within the P limiting range. The use of a N/P ratio to separate N from P limitations provided insight into relationships that would have otherwise have been concealed. Further research should examine the utility of this approach for development of models that link nutrient content and hyperspectral data to photosynthesis at increased scale across a broader range of species.

Acknowledgements

We are grateful to Kendra Newick who assisted with the preparation of the nutrient solutions. The project was partly funded through the Resilient Forests programme, which is funded

through Scion SSIF as well as the Forest Grower's Levy Trust. Funding was also received from the National Institute for Forest Products Innovation (Project Number NIF073-1819), which comprised contributions from the Australian Government, Australasian Forestry Companies and South Australian and Tasmanian State Governments.

References

Aerts, R., & Chapin, F.S. (2000). The mineral nutrition of wild plants revisited: A re-evaluation of processes and patterns. *Advances in Ecological Research, Vol 30* (pp. 1-67)

Asner, G.P., & Martin, R.E. (2008). Spectral and chemical analysis of tropical forests: Scaling from leaf to canopy levels. *Remote Sensing of Environment, 112*, 3958-3970

Asner, G.P., Martin, R.E., Knapp, D.E., Tupayachi, R., Anderson, C., Carranza, L., Martinez, P., Houcheime, M., Sinca, F., & Weiss, P. (2011a). Spectroscopy of canopy chemicals in humid tropical forests. *Remote Sensing of Environment, 115*, 3587-3598

Asner, G.P., Martin, R.E., Tupayachi, R., Emerson, R., Martinez, P., Sinca, F., Powell, G.V.N., Wright, S.J., & Lugo, A.E. (2011b). Taxonomy and remote sensing of leaf mass per area (LMA) in humid tropical forests. *Ecological Applications, 21*, 85-98

Beer, C., Reichstein, M., Tomelleri, E., Ciais, P., Jung, M., Carvalhais, N., Rödenbeck, C., Arain, M.A., Baldocchi, D., & Bonan, G.B. (2010). Terrestrial gross carbon dioxide uptake: global distribution and covariation with climate. *Science, 329*, 834-838

Berger, K., Atzberger, C., Danner, M., D'Urso, G., Mauser, W., Vuolo, F., & Hank, T. (2018). Evaluation of the PROSAIL model capabilities for future hyperspectral model environments: a review study. *Remote Sensing, 10*, 85

Blakemore, L.C., Searl, P.L., & Daly, B.K. (1987). Methods for chemical analysis of soils. *NZ Soil Bureau Scientific Report, 80*, 21-45

Bown, H.E., Mason, E.G., Clinton, P.W., & Watt, M.S. (2009a). Chlorophyll fluorescence response of Pinus radiata clones to nitrogen and phosphorus supply. *Ciencia E Investigacion Agraria, 36*, 451-464

Bown, H.E., Watt, M.S., Clinton, P.W., Mason, E.G., & Richardson, B. (2007). Partititioning concurrent influences of nitrogen and phosphorus supply on photosynthetic model parameters of Pinus radiata. *Tree physiology, 27*, 335-344

704 Bown, H.E., Watt, M.S., Mason, E.G., Clinton, P.W., & Whitehead, D. (2009b). The influence of nitrogen
705 and phosphorus supply and genotype on mesophyll conductance limitations to photosynthesis in
706 *Pinus radiata*. *Tree physiology, 29*, 1143-1151
707 Buddenbaum, H., Pueschel, P., Stellmes, M., Werner, W., & Hill, J. (2011). Measuring water and
708 Chlorophyll content on the leaf and canopy scale. *EARSeL eProc, 10*, 66-72
709 Buddenbaum, H., Stern, O., Paschmionka, B., Hass, E., Gattung, T., Stoffels, J., Hill, J., & Werner, W.
710 (2015). Using VNIR and SWIR field imaging spectroscopy for drought stress monitoring of beech
711 seedlings. *International Journal of Remote Sensing, 36*, 4590-4605
712 Buddenbaum, H., Watt, M.S., Scholten, R.C., & Hill, J. (2019). Preprocessing Ground-Based Visible/Near
713 Infrared Imaging Spectroscopy Data Affected by Smile Effects. *Sensors, 19*, 1543
714 Camino, C., Gonzalez-Dugo, V., Hernandez, P., & Zarco-Tejada, P.J. (2019). Radiative transfer Vcmax
715 estimation from hyperspectral imagery and SIF retrievals to assess photosynthetic performance in
716 rainfed and irrigated plant phenotyping trials. *Remote Sensing of Environment*, 111186
717 Carter, G.A. (1994). Ratios of leaf reflectances in narrow wavebands as indicators of plant stress. *Remote*
718 *sensing, 15*, 697-703
719 Cendrero-Mateo, M.P., Moran, M.S., Papuga, S.A., Thorp, K.R., Alonso, L., Moreno, J., Ponce-Campos,
720 G., Rascher, U., & Wang, G. (2015). Plant chlorophyll fluorescence: active and passive
721 measurements at canopy and leaf scales with different nitrogen treatments. *Journal of*
722 *Experimental Botany, 67*, 275-286
723 Chen, J.M., Leblanc, S.G., Cihlar, J.C., Bicheron, P., Leroy, M., Deering, D., & Eck, T. (1997). Studies of
724 BRDF in conifer and deciduous boreal forests using the 4-scale model and airborne POLDER and
725 ground-based PARABOLA measurements. In (pp. 165-167): IEEE
726 Collatz, G.J., Ball, J.T., Grivet, C., & Berry, J.A. (1991). Physiological and environmental regulation of
727 stomatal conductance, photosynthesis and transpiration: a model that includes a laminar boundary
728 layer. *Agricultural and forest meteorology, 54*, 107-136
729 Colombo, R., Meroni, M., Marchesi, A., Busetto, L., Rossini, M., Giardino, C., & Panigada, C. (2008).
730 Estimation of leaf and canopy water content in poplar plantations by means of hyperspectral
731 indices and inverse modeling. *Remote Sensing of Environment, 112*, 1820-1834
732 Croft, H., Chen, J., & Zhang, Y. (2014). The applicability of empirical vegetation indices for determining
733 leaf chlorophyll content over different leaf and canopy structures. *Ecological Complexity, 17*, 119-
734 130

735 Croft, H., Chen, J.M., Luo, X., Bartlett, P., Chen, B., & Staebler, R.M. (2017). Leaf chlorophyll content as
736 a proxy for leaf photosynthetic capacity. *Global Change Biology, 23*, 3513-3524
737 Curran, P.J., Dungan, J.L., & Peterson, D.L. (2001). Estimating the foliar biochemical concentration of
738 leaves with reflectance spectrometry: testing the Kokaly and Clark methodologies. *Remote Sensing*
739 *of Environment, 76*, 349-359
740 Dechant, B., Cuntz, M., Vohland, M., Schulz, E., & Doktor, D. (2017). Estimation of photosynthesis traits
741 from leaf reflectance spectra: correlation to nitrogen content as the dominant mechanism. *Remote*
742 *Sensing of Environment, 196*, 279-292
743 Dobrowski, S.Z., Pushnik, J.C., Zarco-Tejada, P.J., & Ustin, S.L. (2005). Simple reflectance indices track
744 heat and water stress-induced changes in steady-state chlorophyll fluorescence at the canopy
745 scale. *Remote Sensing of Environment, 97*, 403-414
746 Domingues, T.F., Meir, P., Feldpausch, T.R., Saiz, G., Veenendaal, E.M., Schrodt, F., Bird, M.,
747 Djagbletey, G., Hien, F., & Compaore, H. (2010). Co-limitation of photosynthetic capacity by
748 nitrogen and phosphorus in West Africa woodlands. *Plant, Cell & Environment, 33*, 959-980
749 Doughty, C.E., Asner, G.P., & Martin, R.E. (2011). Predicting tropical plant physiology from leaf and
750 canopy spectroscopy. *Oecologia, 165*, 289-299
751 Drolet, G.G., Middleton, E.M., Huemmrich, K.F., Hall, F.G., Amiro, B.D., Barr, A.G., Black, T.A.,
752 McCaughey, J.H., & Margolis, H.A. (2008). Regional mapping of gross light-use efficiency using
753 MODIS spectral indices. *Remote Sensing of Environment, 112*, 3064-3078
754 Evans, J.R. (1996). Developmental constraints on photosynthesis: effects of light and nutrition.
755 *Photosynthesis and the Environment* (pp. 281-304): Springer
756 Fang, M., Ju, W., Zhan, W., Cheng, T., Qiu, F., & Wang, J. (2017). A new spectral similarity water index
757 for the estimation of leaf water content from hyperspectral data of leaves. *Remote Sensing of*
758 *Environment, 196*, 13-27
759 Farquhar, G.D., von Caemmerer, S., & Berry, J.A. (1980). A biochemical model of photosynthetic CO_2
760 assimilation in leaves of C_3 species. *Planta, 149*, 78-90
761 Féret, J.B., Gitelson, A.A., Noble, S.D., & Jacquemoud, S. (2017). PROSPECT-D: Towards modeling leaf
762 optical properties through a complete lifecycle. *Remote Sensing of Environment, 193*, 204-215
763 Frankenberg, C., Butz, A., & Toon, G.C. (2011). Disentangling chlorophyll fluorescence from atmospheric
764 scattering effects in O2 A-band spectra of reflected sun-light. *Geophysical Research Letters, 38*

765 Fuentes, D.A., Gamon, J.A., Cheng, Y., Claudio, H.C., Qiu, H.-l., Mao, Z., Sims, D.A., Rahman, A.F.,
766 Oechel, W., & Luo, H. (2006). Mapping carbon and water vapor fluxes in a chaparral ecosystem
767 using vegetation indices derived from AVIRIS. *Remote Sensing of Environment, 103*, 312-323
768 Gamon, J., Penuelas, J., & Field, C. (1992). A narrow-waveband spectral index that tracks diurnal
769 changes in photosynthetic efficiency. *Remote Sensing of environment, 41*, 35-44
770 Gamon, J., Serrano, L., & Surfus, J.S. (1997). The photochemical reflectance index: an optical indicator
771 of photosynthetic radiation use efficiency across species, functional types, and nutrient levels.
772 *Oecologia, 112*, 492-501
773 Gamon, J.A., Filella, A., & Penuelas, J. (1993). The Dynamic 531-Nanometer Ä Reflectance Signal: A
774 Survey of Twenty Angiosperm Species, In Photosynthetic Responses to the Environment,
775 American Society of Plant Physiologists, Rockville, MD,
776 USA, 172–177, 1993., 172-177
777 Gamon, J.A., Huemmrich, K.F., Wong, C.Y.S., Ensminger, I., Garrity, S., Hollinger, D.Y., Noormets, A., &
778 Peñuelas, J. (2016). A remotely sensed pigment index reveals photosynthetic phenology in
779 evergreen conifers. *Proceedings of the National Academy of Sciences, 113*, 13087-13092
780 Garbulsky, M.F., Peñuelas, J., Gamon, J., Inoue, Y., & Filella, I. (2011). The photochemical reflectance
781 index (PRI) and the remote sensing of leaf, canopy and ecosystem radiation use efficiencies: A
782 review and meta-analysis. *Remote Sensing of Environment, 115*, 281-297
783 Gastellu-Etchegorry, J.-P., Demarez, V., Pinel, V., & Zagolski, F. (1996). Modeling radiative transfer in
784 heterogeneous 3-D vegetation canopies. *Remote Sensing of Environment, 58*, 131-156
785 Genty, B., Briantais, J., & Baker, N.R. (1989). The relationship between the quantum yield of
786 photosynthetic electron transport and quenching of chlorophyll fluorescence. *Biochimica et*
787 *Biophysica Acta, 990*, 87-92
788 Gillon, D., Houssard, C., & Joffre, R. (1999). Using near-infrared reflectance spectroscopy to predict
789 carbon, nitrogen and phosphorus content in heterogeneous plant material. *Oecologia, 118*, 173-
790 182
791 Gitelson, A.A., Gamon, J.A., & Solovchenko, A. (2017). Multiple drivers of seasonal change in PRI:
792 Implications for photosynthesis 1. Leaf level. *Remote Sensing of Environment, 191*, 110-116
793 Gitelson, A.A., Kaufman, Y.J., & Merzlyak, M.N. (1996). Use of a green channel in remote sensing of
794 global vegetation from EOS-MODIS. *Remote Sensing of Environment, 58*, 289-298

795 Gitelson, A.A., & Merzlyak, M.N. (1996). Signature analysis of leaf reflectance spectra: algorithm
796 development for remote sensing of chlorophyll. *Journal of plant physiology, 148*, 494-500
797 Groenendijk, M., Dolman, A.J., Van der Molen, M.K., Leuning, R., Arneth, A., Delpierre, N., Gash, J.H.C.,
798 Lindroth, A., Richardson, A.D., & Verbeeck, H. (2011). Assessing parameter variability in a
799 photosynthesis model within and between plant functional types using global Fluxnet eddy
800 covariance data. *Agricultural and forest meteorology, 151*, 22-38
801 Guanter, L., Kaufmann, H., Segl, K., Foerster, S., Rogass, C., Chabrillat, S., Kuester, T., Hollstein, A.,
802 Rossner, G., & Chlebek, C. (2015). The EnMAP spaceborne imaging spectroscopy mission for
803 earth observation. *Remote Sensing, 7*, 8830-8857
804 Guanter, L., Zhang, Y., Jung, M., Joiner, J., Voigt, M., Berry, J.A., Frankenberg, C., Huete, A.R., Zarco-
805 Tejada, P., & Lee, J.-E. (2014). Global and time-resolved monitoring of crop photosynthesis with
806 chlorophyll fluorescence. *Proceedings of the National Academy of Sciences, 111*, E1327-E1333
807 Guo, J., & Trotter, C.M. (2004). Estimating photosynthetic light-use efficiency using the photochemical
808 reflectance index: variations among species. *Functional Plant Biology, 31*, 255-265
809 Hernández-Clemente, R., Navarro-Cerrillo, R.M., Suárez, L., Morales, F., & Zarco-Tejada, P.J. (2011).
810 Assessing structural effects on PRI for stress detection in conifer forests. *Remote Sensing of*
811 *Environment, 115*, 2360-2375
812 Hernández-Clemente, R., Navarro-Cerrillo, R.M., & Zarco-Tejada, P.J. (2012). Carotenoid content
813 estimation in a heterogeneous conifer forest using narrow-band indices and PROSPECT+ DART
814 simulations. *Remote Sensing of Environment, 127*, 298-315
815 Hernández-Clemente, R., Navarro-Cerrillo, R.M., & Zarco-Tejada, P.J. (2014). Deriving predictive
816 relationships of carotenoid content at the canopy level in a conifer forest using hyperspectral
817 imagery and model simulation. *IEEE Transactions on Geoscience and Remote Sensing, 52*, 5206-
818 5217
819 Hilker, T., Coops, N.C., Hall, F.G., Black, T.A., Chen, B., Krishnan, P., Wulder, M.A., Sellers, P.J.,
820 Middleton, E.M., & Huemmrich, K.F. (2008). A modeling approach for upscaling gross ecosystem
821 production to the landscape scale using remote sensing data. *Journal of Geophysical Research:*
822 *Biogeosciences, 113*
823 Hill, J., Buddenbaum, H., & Townsend, P.A. (2019). Imaging Spectroscopy of Forest Ecosystems:
824 Perspectives for the Use of Space-borne Hyperspectral Earth Observation Systems. *Surveys in*
825 *Geophysics, 40*, 553-588

826 Holden, M. (1965). Chlorophylls. In T.W. Goodwin (Ed.), *Chemistry and Biochemistry of Plant Pigments*
827 (pp. 641-688). London: Academic Press
828 Horler, D.N.H., Dockray, M., Barber, J., & Barringer, A.R. (1983). Red edge measurements for remotely
829 sensing plant chlorophyll content. *Advances in Space Research, 3*, 273-277
830 Houborg, R., Cescatti, A., Migliavacca, M., & Kustas, W.P. (2013). Satellite retrievals of leaf chlorophyll
831 and photosynthetic capacity for improved modeling of GPP. *Agricultural and forest meteorology,*
832 *177*, 10-23
833 Ingestad, T. (1971). A definition of optimum nutrient requirements in Birch Seedlings. II. *Physiologia*
834 *plantarum, 24*, 118-125
835 Ingestad, T. (1979). Mineral nutrient requirements of *Pinus silvestris* and *Picea abies* seedlings.
836 *Physiologia plantarum, 45*, 373-380
837 Ingestad, T., & Lund, A. (1986). New concepts on soil fertility and plant nutrition as illustrated by research
838 on forest trees and stands. *Geoderma, 40*, 237-252
839 Jacquemoud, S., & Baret, F. (1990). PROSPECT: A model of leaf optical properties spectra. *Remote*
840 *Sensing of Environment, 34*, 75-91
841 Jacquemoud, S., Verhoef, W., Baret, F., Bacour, C., Zarco-Tejada, P.J., Asner, G.P., François, C., &
842 Ustin, S.L. (2009). PROSPECT + SAIL models: A review of use for vegetation characterization.
843 *Remote Sensing of Environment, 113*, S56-S66
844 Jay, S., Bendoula, R., Hadoux, X., Féret, J.-B., & Gorretta, N. (2016). A physically-based model for
845 retrieving foliar biochemistry and leaf orientation using close-range imaging spectroscopy. *Remote*
846 *Sensing of Environment, 177*, 220-236
847 Kattenborn, T., Schiefer, F., Zarco-Tejada, P., & Schmidtlein, S. (2019). Advantages of retrieving pigment
848 content [µg/cm2] versus concentration [%] from canopy reflectance. *Remote Sensing of*
849 *Environment, 230*, 111195
850 Kattge, J., & Knorr, W. (2007). Temperature acclimation in a biochemical model of photosynthesis: a
851 reanalysis of data from 36 species. *Plant, Cell & Environment, 30*, 1176-1190
852 Knecht, M.F., & Göransonn, A. (2004). Terrestrial plants require nutrients in similar proportions. *Tree*
853 *physiology, 24*, 447-460
854 Le Maire, G., François, C., Soudani, K., Berveiller, D., Pontailler, J.-Y., Bréda, N., Genet, H., Davi, H., &
855 Dufrêne, E. (2008). Calibration and validation of hyperspectral indices for the estimation of

broadleaved forest leaf chlorophyll content, leaf mass per area, leaf area index and leaf canopy biomass. *Remote Sensing of Environment, 112*, 3846-3864

Leuning, R. (1995). A critical appraisal of a combined stomatal-photosynthesis model for C3 plants. *Plant, Cell and Environment, 18*, 339-355

Leuning, R. (1997). Scaling to a common temperature improves the correlation between the photosynthesis parameters J max and V cmax. *Journal of Experimental Botany, 48*, 345-347

Long, S.P., & Bernacchi, C.J. (2003). Gas exchange measurements, what can they tell us about the underlying limitations to photosynthesis? Procedures and sources of error. *Journal of Experimental Botany, 54*, 2393-2401

Luther, J.E., & Carroll, A.L. (1999). Development of an index of balsam fir vigor by foliar spectral reflectance. *Remote Sensing of Environment, 69*, 241-252

Malenovský, Z., Albrechtová, J., Lhotáková, Z., Zurita-Milla, R., Clevers, J., Schaepman, M.E., & Cudlín, P. (2006). Applicability of the PROSPECT model for Norway spruce needles. *International Journal of Remote Sensing, 27*, 5315-5340

Marschner, H. (1995). *Mineral nutrition of higher plants*. (2nd ed.). London: Academic Press

Masaitis, G., Mozgeris, G., & Augustaitis, A. (2014). Estimating crown defoliation and the chemical constituents in needles of Scots pine (Pinus sylvestris L.) trees by laboratory acquired hyperspectral data. *Balt. For, 20*, 314-325

Mead, D.J. (2013). *Sustainable management of Pinus radiata plantations*. Food and agriculture organization of the United nations (FAO)

Medlyn, B.E., Dreyer, E., Ellsworth, D., Forstreuter, M., Harley, P.C., Kirschbaum, M.U.F., Le Roux, X., Montpied, P., Strassemeyer, J., & Walcroft, A. (2002). Temperature response of parameters of a biochemically based model of photosynthesis. II. A review of experimental data. *Plant, Cell & Environment, 25*, 1167-1179

Meroni, M., Rossini, M., Guanter, L., Alonso, L., Rascher, U., Colombo, R., & Moreno, J. (2009). Remote sensing of solar-induced chlorophyll fluorescence: Review of methods and applications. *Remote Sensing of Environment, 113*, 2037-2051

Middleton, E.M., Cheng, Y.-B., Hilker, T., Black, T.A., Krishnan, P., Coops, N.C., & Huemmrich, K.F. (2009). Linking foliage spectral responses to canopy-level ecosystem photosynthetic light-use efficiency at a Douglas-fir forest in Canada. *Canadian Journal of Remote Sensing, 35*, 166-188

886 Mohammed, G.H., Colombo, R., Middleton, E.M., Rascher, U., van der Tol, C., Nedbal, L., Goulas, Y.,
887 Pérez-Priego, O., Damm, A., & Meroni, M. (2019). Remote sensing of solar-induced chlorophyll
888 fluorescence (SIF) in vegetation: 50 years of progress. *Remote Sensing of Environment, 231*,
889 111177
890 Mouazen, A.M., Kuang, B., De Baerdemaeker, J., & Ramon, H. (2010). Comparison among principal
891 component, partial least squares and back propagation neural network analyses for accuracy of
892 measurement of selected soil properties with visible and near infrared spectroscopy. *Geoderma,*
893 *158*, 23-31
894 Nichol, C.J., Huemmrich, K.F., Black, T.A., Jarvis, P.G., Walthall, C.L., Grace, J., & Hall, F.G. (2000).
895 Remote sensing of photosynthetic-light-use efficiency of boreal forest. *Agricultural and forest*
896 *meteorology, 101*, 131-142
897 Niinemets, Ü., & Sack, L. (2006). Structural determinants of leaf light-harvesting capacity and
898 photosynthetic potentials. *Progress in botany* (pp. 385-419): Springer
899 Niinemets, Ü., & Tenhunen, J.D. (1997). A model separating leaf structural and physiological effects on
900 carbon gain along light gradients for the shade-tolerant species Acer saccharum. *Plant, Cell &*
901 *Environment, 20*, 845-866
902 North, P.R.J. (1996). Three-dimensional forest light interaction model using a Monte Carlo method. *IEEE*
903 *Transactions on Geoscience and Remote Sensing, 34*, 946-956
904 NZFOA (2018). 2018 Facts and Figures. New Zealand Plantation Forest Industry. New Zealand Forest
905 Owners Association, Wellington, 35 pp
906 Penuelas, J., Filella, I., & Gamon, J.A. (1995). Assessment of photosynthetic radiation-use efficiency with
907 spectral reflectance. *New Phytologist, 131*, 291-296
908 Peñuelas, J., Garbulsky, M.F., & Filella, I. (2011). Photochemical reflectance index (PRI) and remote
909 sensing of plant CO2 uptake. *New Phytologist, 191*, 596-599
910 Petisco, C., García-Criado, B., De Aldana, B.R.V., Zabalgogeazcoa, I., & Mediavilla, S. (2005). Use of
911 near-infrared reflectance spectroscopy in predicting nitrogen, phosphorus and calcium contents in
912 heterogeneous woody plant species. *Analytical and bioanalytical chemistry, 382*, 458-465
913 Porcar-Castell, A., Tyystjärvi, E., Atherton, J., Van der Tol, C., Flexas, J., Pfündel, E.E., Moreno, J.,
914 Frankenberg, C., & Berry, J.A. (2014). Linking chlorophyll a fluorescence to photosynthesis for
915 remote sensing applications: mechanisms and challenges. *Journal of Experimental Botany, 65*,
916 4065-4095

Porder, S., Asner, G.P., & Vitousek, P.M. (2005). Ground-based and remotely sensed nutrient availability across a tropical landscape. *Proceedings of the National Academy of Sciences, 102*, 10909-10912

Prikaziuk, E., & van der Tol, C. (2019). Global Sensitivity Analysis of the SCOPE Model in Sentinel-3 Bands: Thermal Domain Focus. *Remote Sensing, 11*, 2424

R Development Core Team (2011). R: A language and environment for statistical computing. R Foundation for Statistical Computing, Vienna, Austria

Raison, R.J., & Myers, B.J. (1992). The Biology of Forest Growth experiment : linking water and nitrogen availability to the growth of *Pinus radiata*. *Forest Ecology and Management*

Rascher, U., Alonso, L., Burkart, A., Cilia, C., Cogliati, S., Colombo, R., Damm, A., Drusch, M., Guanter, L., & Hanus, J. (2015). Sun-induced fluorescence–a new probe of photosynthesis: First maps from the imaging spectrometer HyPlant. *Global Change Biology, 21*, 4673-4684

Rascher, U., & Pieruschka, R. (2008). Spatio-temporal variations of photosynthesis: the potential of optical remote sensing to better understand and scale light use efficiency and stresses of plant ecosystems. *Precision Agriculture, 9*, 355-366

Reich, P.B., & Schoettle, A.W. (1988). Role of phosphorus and nitrogen in photosynthetic and whole plant carbon gain and nutrient use efficiency in eastern white pine. *Oecologia, 77*, 25-33

Riaño, D., Vaughan, P., Chuvieco, E., Zarco-Tejada, P.J., & Ustin, S.L. (2005). Estimation of fuel moisture content by inversion of radiative transfer models to simulate equivalent water thickness and dry matter content: Analysis at leaf and canopy level. *IEEE Transactions on Geoscience and Remote Sensing, 43*, 819-826

Ripullone, F., Rivelli, A.R., Baraldi, R., Guarini, R., Guerrieri, R., Magnani, F., Peñuelas, J., Raddi, S., & Borghetti, M. (2011). Effectiveness of the photochemical reflectance index to track photosynthetic activity over a range of forest tree species and plant water statuses. *Functional Plant Biology, 38*, 177-186

Rock, B.N., Hoshizaki, T., & Miller, J.R. (1988). Comparison of in situ and airborne spectral measurements of the blue shift associated with forest decline. *Remote Sensing of Environment, 24*, 109-127

Schlerf, M., Atzberger, C., Hill, J., Buddenbaum, H., Werner, W., & Schüler, G. (2010). Retrieval of chlorophyll and nitrogen in Norway spruce (Picea abies L. Karst.) using imaging spectroscopy. *International Journal of Applied Earth Observation and Geoinformation, 12*, 17-26

947 Scholten, R.C., Hill, J., Werner, W., Buddenbaum, H., Dash, J.P., Gallego, M.G., Rolando, C.A., Pearse,
948 G.D., Hartley, R., & Estarija, H.J. (2019). Hyperspectral VNIR-spectroscopy and imagery as a tool
949 for monitoring herbicide damage in wilding conifers. *Biological Invasions, 21*, 3395-3413
950 Sellers, P.J., Berry, J.A., Collatz, G.J., Field, C.B., & Hall, F.G. (1992). Canopy reflectance,
951 photosynthesis, and transpiration. III. A reanalysis using improved leaf models and a new canopy
952 integration scheme. *Remote Sensing of Environment, 42*, 187-216
953 Serbin, S.P., Singh, A., McNeil, B.E., Kingdon, C.C., & Townsend, P.A. (2014). Spectroscopic
954 determination of leaf morphological and biochemical traits for northern temperate and boreal tree
955 species. *Ecological Applications, 24*, 1651-1669
956 Sheriff, D.W., Nambiar, E.K.S., & Fife, D.N. (1986). Relationships between nutrient status, carbon
957 assimilation and water use efficiency in Pinus radiata (D. Don) needles. *Tree physiology, 2*, 73-88
958 Smith, W.K., Biederman, J.A., Scott, R.L., Moore, D.J.P., He, M., Kimball, J.S., Yan, D., Hudson, A.,
959 Barnes, M.L., & MacBean, N. (2018). Chlorophyll fluorescence better captures seasonal and
960 interannual gross primary productivity dynamics across dryland ecosystems of southwestern North
961 America. *Geophysical Research Letters, 45*, 748-757
962 Stein, B.R., Thomas, V.A., Lorentz, L.J., & Strahm, B.D. (2014). Predicting macronutrient concentrations
963 from loblolly pine leaf reflectance across local and regional scales. *GIScience & remote sensing,*
964 *51*, 269-287
965 Stylinski, C.D., Oechel, W.C., Gamon, J.A., Tissue, D.T., Miglietta, F., & Raschi, A. (2000). Effects of
966 lifelong [CO2] enrichment on carboxylation and light utilization of Quercus pubescens Willd.
967 examined with gas exchange, biochemistry and optical techniques. *Plant, Cell & Environment, 23*,
968 1353-1362
969 Suárez, L., Zarco-Tejada, P.J., Berni, J.A.J., González-Dugo, V., & Fereres, E. (2009). Modelling PRI for
970 water stress detection using radiative transfer models. *Remote Sensing of Environment, 113*, 730-
971 744
972 Suárez, L., Zarco-Tejada, P.J., Sepulcre-Cantó, G., Pérez-Priego, O., Miller, J.R., Jiménez-Muñoz, J.C.,
973 & Sobrino, J. (2008). Assessing canopy PRI for water stress detection with diurnal airborne
974 imagery. *Remote Sensing of Environment, 112*, 560-575
975 Taiz, L., Zeiger, E., Møller, I.M., & Murphy, A. (2015). Plant physiology and development
976 Tsay, M.-L., Gjerstad, D.H., & Glover, G.R. (1982). Tree leaf reflectance: a promising technique to rapidly
977 determine nitrogen and chlorophyll content. *Canadian Journal of Forest Research, 12*, 788-792

978 Vasques, G.M., Grunwald, S., & Sickman, J.O. (2008). Comparison of multivariate methods for inferential
979 modeling of soil carbon using visible/near-infrared spectra. *Geoderma, 146*, 14-25
980 Verhoef, W. (1984). Light scattering by leaf layers with application to canopy reflectance modeling: The
981 SAIL model. *Remote Sensing of Environment, 16*, 125-141
982 Verhoef, W., Jia, L., Xiao, Q., & Su, Z. (2007). Unified Optical-Thermal Four-Stream Radiative Transfer
983 Theory for Homogeneous Vegetation Canopies. *IEEE Transactions on Geoscience and Remote*
984 *Sensing, 45*, 1808-1822
985 Verrelst, J., Rivera, J.P., van der Tol, C., Magnani, F., Mohammed, G., & Moreno, J. (2015). Global
986 sensitivity analysis of the SCOPE model: what drives simulated canopy-leaving sun-induced
987 fluorescence? *Remote Sensing of Environment, 166*, 8-21
988 Vogelmann, T.C. (1993). Plant tissue optics. *Annual review of plant biology, 44*, 231-251
989 Walcroft, A.S., Whitehead, D., Silvester, W.B., & Kelliher, F.M. (1997). The response of photosynthetic
990 model parameters to temperature and nitrogen concentration in Pinus radiata D. Don. *Plant, Cell*
991 *and Environment, 20*, 1338-1348
992 Walker, A.P., Beckerman, A.P., Gu, L., Kattge, J., Cernusak, L.A., Domingues, T.F., Scales, J.C.,
993 Wohlfahrt, G., Wullschleger, S.D., & Woodward, F.I. (2014). The relationship of leaf photosynthetic
994 traits–Vcmax and Jmax–to leaf nitrogen, leaf phosphorus, and specific leaf area: a meta-analysis
995 and modeling study. *Ecology and evolution, 4*, 3218-3235
996 Wang, Z., Skidmore, A.K., Darvishzadeh, R., & Wang, T. (2018). Mapping forest canopy nitrogen content
997 by inversion of coupled leaf-canopy radiative transfer models from airborne hyperspectral imagery.
998 *Agricultural and forest meteorology, 253*, 247-260
999 Wang, Z., Skidmore, A.K., Wang, T., Darvishzadeh, R., & Hearne, J. (2015). Applicability of the
1000 PROSPECT model for estimating protein and cellulose+ lignin in fresh leaves. *Remote Sensing of*
1001 *Environment, 168*, 205-218
1002 Watt, M.S., Coker, G., Clinton, P.W., Davis, M.R., Parfitt, R., Simcock, R., Garret, L., Payn, T.W.,
1003 Richardson, B., & Dunningham, A. (2005). Defining sustainability of plantation forests through
1004 identification of site quality indicators influencing productivity- a national view for New Zealand.
1005 *Forest Ecology and Management, 216*, 51-63
1006 Watt, M.S., Davis, M.R., & Parfitt, R.L. (2009). Improved nutritional status of Cupressus lusitanica when
1007 grown adjacent to Pinus radiata. *Canadian Journal of Forest Research-Revue Canadienne De*
1008 *Recherche Forestiere, 39*, 882-887

1009 Watt, M.S., Pearse, G.D., Dash, J.P., Melia, N., & Leonardo, E.M.C. (2019). Application of remote
1010 sensing technologies to identify impacts of nutritional deficiencies on forests. *ISPRS Journal of*
1011 *Photogrammetry and Remote Sensing, 149*, 226-241
1012 Weis, E., & Berry, J.A. (1987). Quantum efficiency of photosystem II in relation to 'energy'-dependent
1013 quenching of chlorophyll fluorescence. *Biochimica et Biophysica Acta (BBA)-Bioenergetics, 894*,
1014 198-208
1015 Wong, C.Y.S., & Gamon, J.A. (2015a). The photochemical reflectance index provides an optical indicator
1016 of spring photosynthetic activation in evergreen conifers. *New Phytologist, 206*, 196-208
1017 Wong, C.Y.S., & Gamon, J.A. (2015b). Three causes of variation in the photochemical reflectance index
1018 (PRI) in evergreen conifers. *New Phytologist, 206*, 187-195
1019 Xu, L., & Baldocchi, D.D. (2003). Seasonal trends in photosynthetic parameters and stomatal
1020 conductance of blue oak (Quercus douglasii) under prolonged summer drought and high
1021 temperature. *Tree physiology, 23*, 865-877
1022 Yoder, B.J., & Pettigrew-Crosby, R.E. (1995). Predicting nitrogen and chlorophyll content and
1023 concentrations from reflectance spectra (400–2500 nm) at leaf and canopy scales. *Remote*
1024 *Sensing of Environment, 53*, 199-211
1025 Zarco-Tejada, P.J., Camino, C., Beck, P.S.A., Calderon, R., Hornero, A., Hernández-Clemente, R.,
1026 Kattenborn, T., Montes-Borrego, M., Susca, L., & Morelli, M. (2018). Previsual symptoms of Xylella
1027 fastidiosa infection revealed in spectral plant-trait alterations. *Nature Plants, 4*, 432-439
1028 Zarco-Tejada, P.J., Catalina, A., González, M.R., & Martín, P. (2013a). Relationships between net
1029 photosynthesis and steady-state chlorophyll fluorescence retrieved from airborne hyperspectral
1030 imagery. *Remote Sensing of Environment, 136*, 247-258
1031 Zarco-Tejada, P.J., González-Dugo, M.V., & Fereres, E. (2016). Seasonal stability of chlorophyll
1032 fluorescence quantified from airborne hyperspectral imagery as an indicator of net photosynthesis
1033 in the context of precision agriculture. *Remote Sensing of Environment, 179*, 89-103
1034 Zarco-Tejada, P.J., González-Dugo, V., Williams, L.E., Suárez, L., Berni, J.A.J., Goldhamer, D., &
1035 Fereres, E. (2013b). A PRI-based water stress index combining structural and chlorophyll effects:
1036 Assessment using diurnal narrow-band airborne imagery and the CWSI thermal index. *Remote*
1037 *Sensing of Environment, 138*, 38-50
1038 Zarco-Tejada, P.J., Hornero, A., Beck, P.S.A., Kattenborn, T., Kempeneers, P., & Hernández-Clemente,
1039 R. (2019). Chlorophyll content estimation in an open-canopy conifer forest with Sentinel-2A and

hyperspectral imagery in the context of forest decline. *Remote Sensing of Environment, 223*, 320-335

Zarco-Tejada, P.J., Miller, J.R., Harron, J., Hu, B., Noland, T.L., Goel, N., Mohammed, G.H., & Sampson, P. (2004a). Needle chlorophyll content estimation through model inversion using hyperspectral data from boreal conifer forest canopies. *Remote Sensing of Environment, 89*, 189-199

Zarco-Tejada, P.J., Miller, J.R., Morales, A., Berjón, A., & Agüera, J. (2004b). Hyperspectral indices and model simulation for chlorophyll estimation in open-canopy tree crops. *Remote Sensing of Environment, 90*, 463-476

Zarco-Tejada, P.J., Miller, J.R., Noland, T.L., Mohammed, G.H., & Sampson, P.H. (2001). Scaling-up and model inversion methods with narrowband optical indices for chlorophyll content estimation in closed forest canopies with hyperspectral data. *IEEE Transactions on Geoscience and Remote Sensing, 39*, 1491-1507

Zhang, Q., Xiao, X., Braswell, B., Linder, E., Baret, F., & Moore Iii, B. (2005). Estimating light absorption by chlorophyll, leaf and canopy in a deciduous broadleaf forest using MODIS data and a radiative transfer model. *Remote Sensing of Environment, 99*, 357-371

List of figure captions

Figure 1. Images of individual trees selected from the treatments (left) and their corresponding canopy reflectance (right).

Figure 2. Relationships between mass based nitrogen and phosphorus. The treatment designation for individual trees are denoted by filled circles while treatment means area shown as large crosses with differing colours. The dashed line in panel (a) represents a N/P ratio of 10. Values of foliage N and P content above the line are N limited while those below the line are P limited.

Figure 3. Tree level variation in (a) canopy reflectance and (b) the 1st derivative of canopy reflectance against wavelength. Treatment identity is identified by lines with differing colours.

Figure 4. Variation in (a, e) canopy reflectance across the entire spectrum and between (b, f) 400 – 500 nm, (c, g) 500 – 600 nm and (d, h) 600 – 700 nm for data averaged by (a – d) treatment and (e – h) limitation type.

Figure 5. Variation in treatment significance, as indicated by the *P*-value, for reflectance (open red circles) and the first derivative of reflectance (filled blue circles). The grey region shown at the top of the figure outlines the area of insignificance at $P > 0.05$ while the dashed line is drawn at $P = 0.001$. The y-axis is shown as a logarithmic scale to highlight the significance strength.

Figure 6. Variation in treatment significance, as indicated by the *P*-value, for (a) reflectance and (b) the first derivative of reflectance, for comparisons of P under low (red circles) and high N (blue circles) and comparisons of N under low (green circles) and high P (black circles). The grey region shown at the top of the figure outlines the area of insignificance at $P > 0.0125$ while

the dashed line is drawn at $P = 0.001$. The y-axis is shown as a logarithmic scale to highlight the significance strength.

Figure 7. Relationships between nitrogen and phosphorus content and (a, b) Photochemical Reflectance Index and (c, d) Sun Induced Chlorophyll Fluorescence, under N (open brown circles) and P limiting conditions (filled teal circles). Lines have been fitted to relationships that are significant at $P < 0.048$ with the brown and teal lines fitted respectively to N and P limited data.

Figure 8. Relationships between measured chlorophyll$_{a+b}$ and inverted chlorophyll$_{a+b}$ and (a, b) V_{cmax} and (c, d) J_{max} under N (open brown circles) and P limiting conditions (filled teal circles). Lines have been fitted to relationships that are significant at $P < 0.05$ with the brown lines fitted to N limited data.

Figure 9. Relationships between area based nitrogen and phosphorus and (a, b) V_{cmax} and (c, d) J_{max} under N (open brown circles) and P limiting conditions (filled teal circles). Lines have been fitted to relationships that are significant at $P < 0.05$ with the brown and teal lines fitted respectively to N and P limited data.

Figure 10. Relationship between measured chlorophyll and estimated chlorophyll derived from the PROSAIL inversion. The 1:1 line is shown as a solid line and treatments are denoted by filled circles with differing colours.

Figure 11. Relationships between Photochemical Reflectance Index and Sun Induced Chlorophyll Fluorescence and (a, b) V_{cmax} and (c, d) J_{max} under N (open brown circles) and P

limiting conditions (filled teal circles). The black lines were fitted to the combined N and P limited dataset.

1112 Table 1. Model parameters used within PROSAIL.
1113

Variable parameters				
Parameter	Symbol	Unit	Min	Max
Mesophyll structure parameter	N		1.4	1.6
Chlorophyll a+b	Chl_{a+b}	µg cm^{-2}	25	60
Carotenoids	C_{cx}	µg cm^{-2}	1	15
Anthocyanins	C_{anth}	µg cm^{-2}	0	5
Water content	C_w	g cm^{-2}	0.0002	0.06
Dry matter content	C_m	g cm^{-2}	0.0001	0.03
Average leaf inclination angle	ALA (LIDFa)	°	0	90
Leaf area index	LAI		0.5	5

Fixed parameters			
Parameter	Symbol	Unit	Value
Brown pigments	C_{bp}		0
Hot spot parameter	*Hot*		0.1
Observation zenith angle	θ_o	°	0
Illumination zenith angle	θ_s	°	45
Relative azimuth angle	ψ	°	0

1114

Table 2. Summary of model precision, as denoted by the coefficient of determination (R^2) for models describing the maximal carboxylation capacity (V_{cmax}) and the maximal electron transport rate (J_{max}). Measured predictors include area based measurements of nitrogen (N), phosphorus (P) and chlorophyll (Chl_{a+b}). Predictors that were derived from hyperspectral data included Photochemical Reflectance Index (PRI), Sun-Induced Chlorophyll Fluorescence (SIF) and chlorophyll derived from the PROSAIL inversion ($Chl_{a+b\ PROSAIL}$).

Predictor(s)	All data		N limiting		P limiting	
	V_{cmax}	J_{max}	V_{cmax}	J_{max}	V_{cmax}	J_{max}
Measured variables						
N	0.84***	0.82***	0.82***	0.87***	0.01^{ns}	0.02^{ns}
P	0.04^{ns}	0.06^{ns}	0.33^{ns}	0.31^{ns}	0.50*	0.58*
Chl_{a+b}	0.85***	0.82***	0.85***	0.86***	0.02^{ns}	0.01^{ns}
Derived predictors						
$Chl_{a+b\ PROSAIL}$	0.79***	0.76***	0.64***	0.63***	0.03^{ns}	0.04^{ns}
SIF	0.78***	0.80***	0.69***	0.70***	0.35^{ns}	0.68**
PRI	0.84***	0.84***	0.73***	0.75***	0.42^{ns}	0.51*

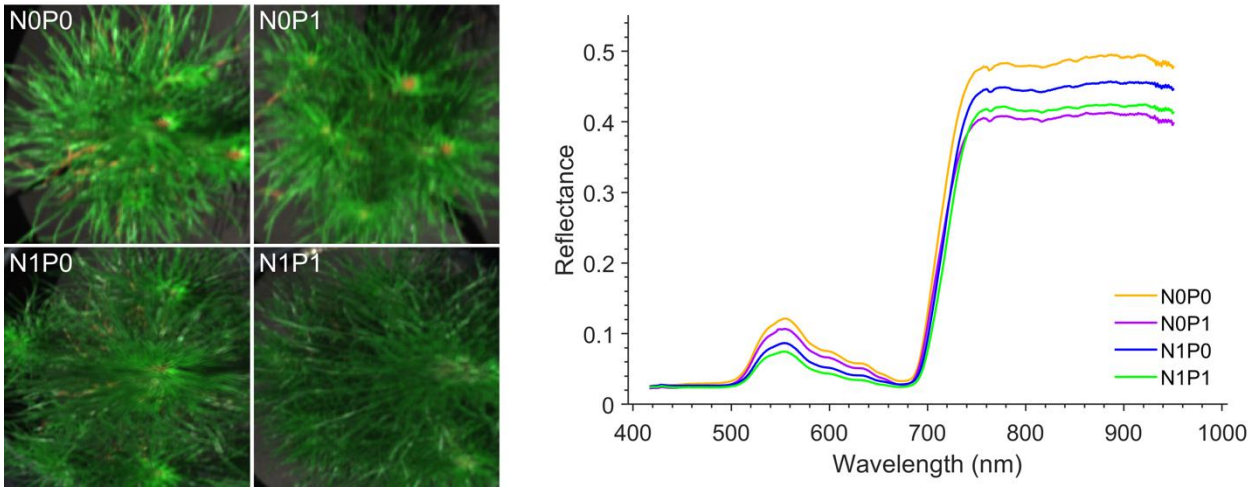

Figure 1. Images of individual trees selected from the treatments (left) and their corresponding canopy reflectance (right).

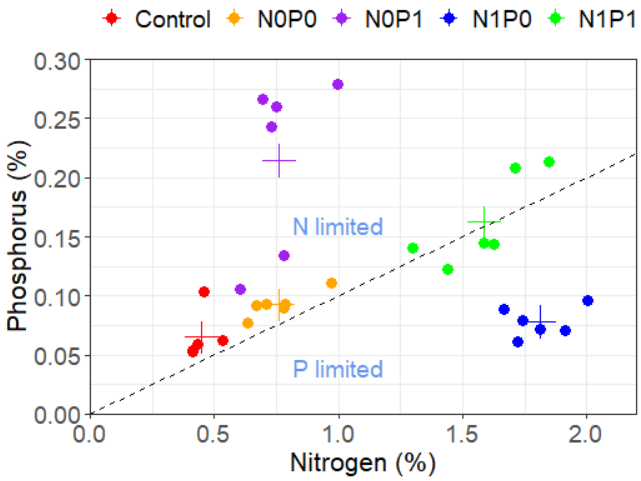

Figure 2. Relationships between mass based nitrogen and phosphorus. The treatment designation for individual trees are denoted by filled circles while treatment means area shown as large crosses with differing colours. The dashed line in panel (a) represents a N/P ratio of 10. Values of foliage N and P content above the line are N limited while those below the line are P limited.

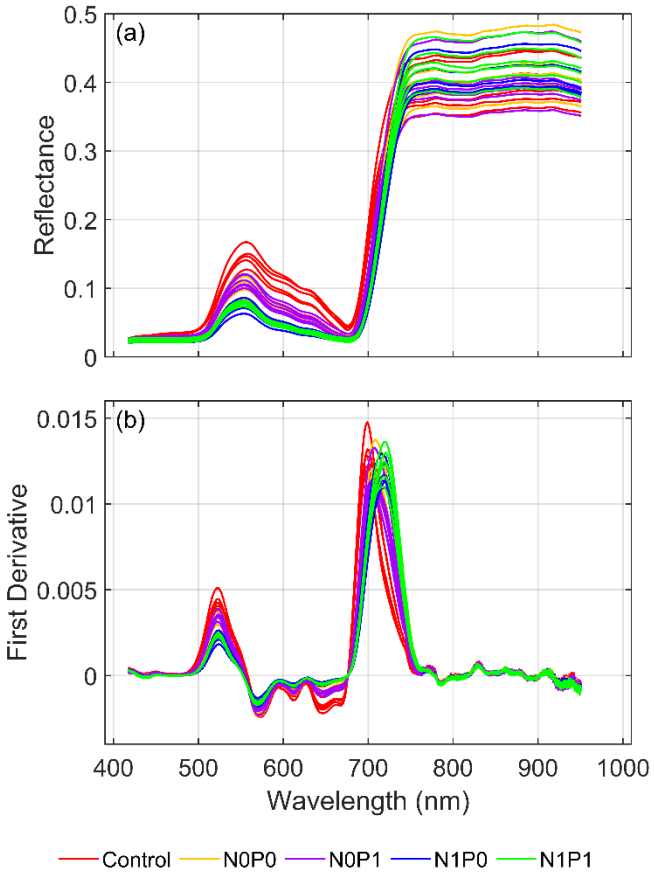

1151

1152 Figure 3. Tree level variation in (a) canopy reflectance and (b) the 1st derivative of canopy

1153 reflectance against wavelength. Treatment identity is identified by lines with differing colours.

1154

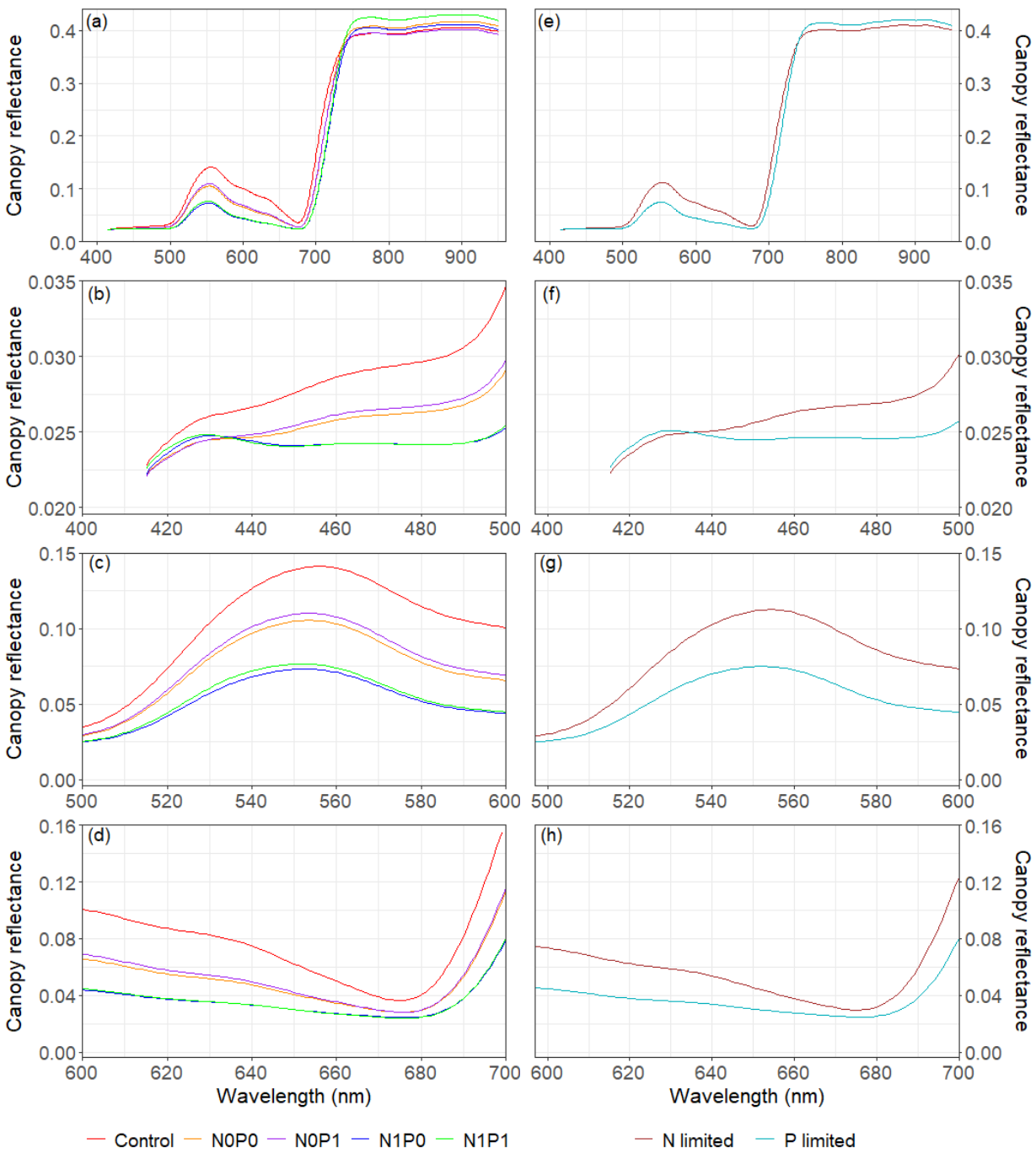

Figure 4. Variation in (a, e) canopy reflectance across the entire spectrum and between (b, f) 400 – 500 nm, (c, g) 500 – 600 nm and (d, h) 600 – 700 nm for data averaged by (a – d) treatment and (e – h) limitation type.

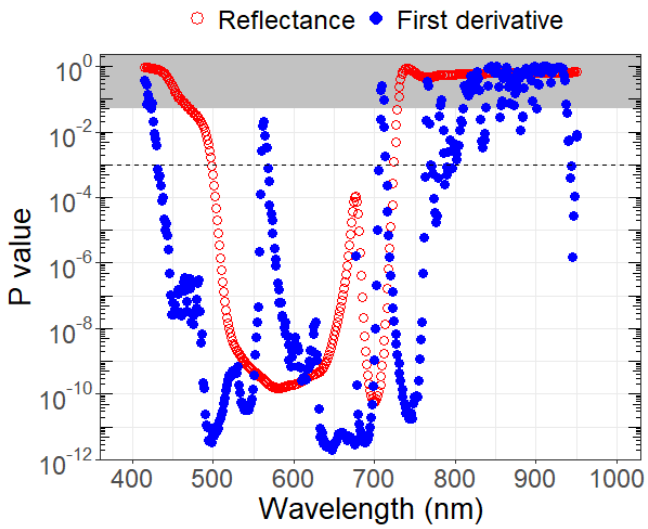

Figure 5. Variation in treatment significance, as indicated by the *P*-value, for reflectance (open red circles) and the first derivative of reflectance (filled blue circles). The grey region shown at the top of the figure outlines the area of insignificance at $P > 0.05$ while the dashed line is drawn at $P = 0.001$. The y-axis is shown as a logarithmic scale to highlight the significance strength.

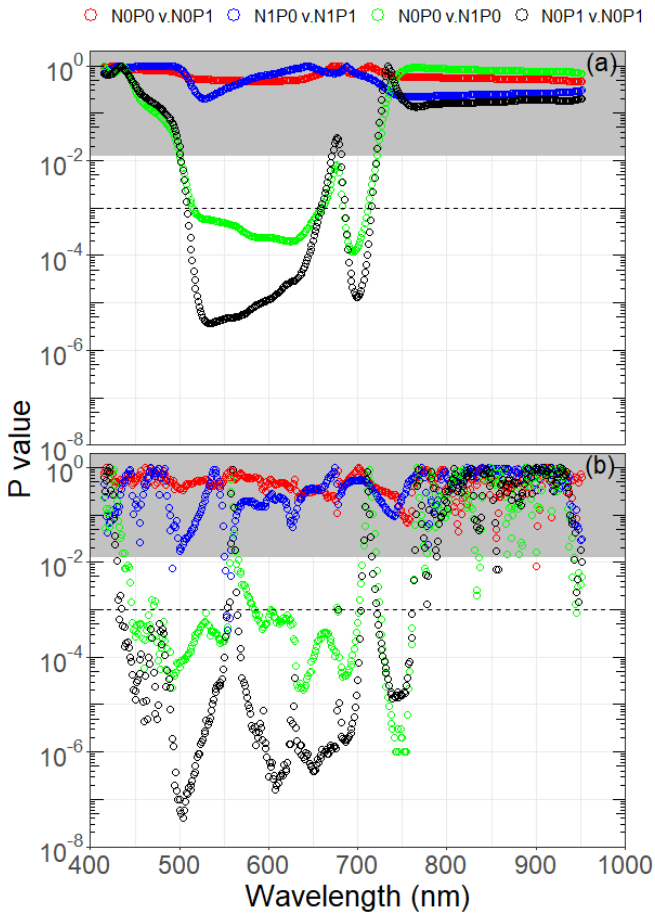

Figure 6. Variation in treatment significance, as indicated by the *P*-value, for (a) reflectance and (b) the first derivative of reflectance, for comparisons of P under low (red circles) and high N (blue circles) and comparisons of N under low (green circles) and high P (black circles). The grey region shown at the top of the figure outlines the area of insignificance at $P > 0.0125$ while the dashed line is drawn at $P = 0.001$. The y-axis is shown as a logarithmic scale to highlight the significance strength.

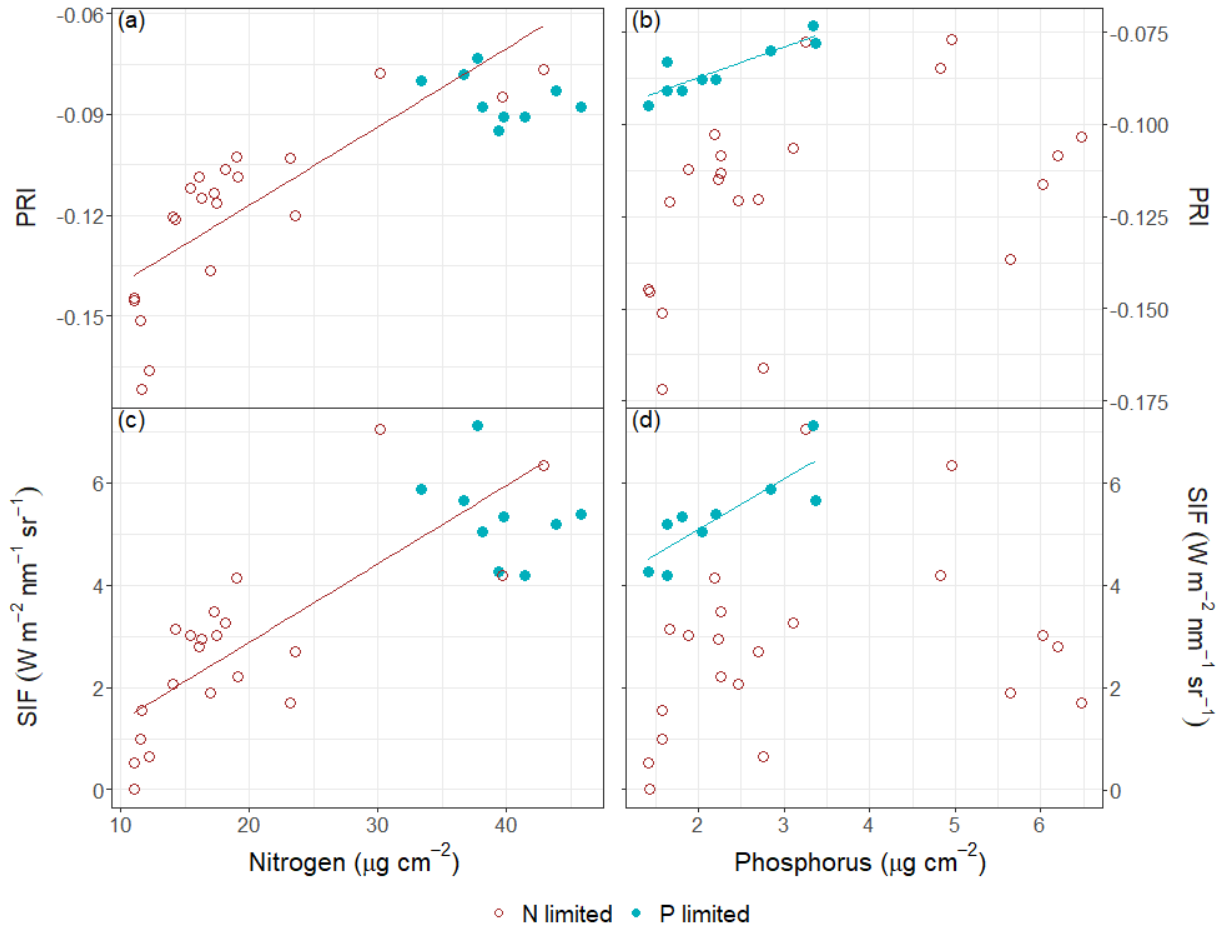

Figure 7. Relationships between nitrogen and phosphorus content and (a, b) Photochemical Reflectance Index and (c, d) Sun Induced Chlorophyll Fluorescence, under N (open brown circles) and P limiting conditions (filled teal circles). Lines have been fitted to relationships that are significant at P <0.048 with the brown and teal lines fitted respectively to N and P limited data.

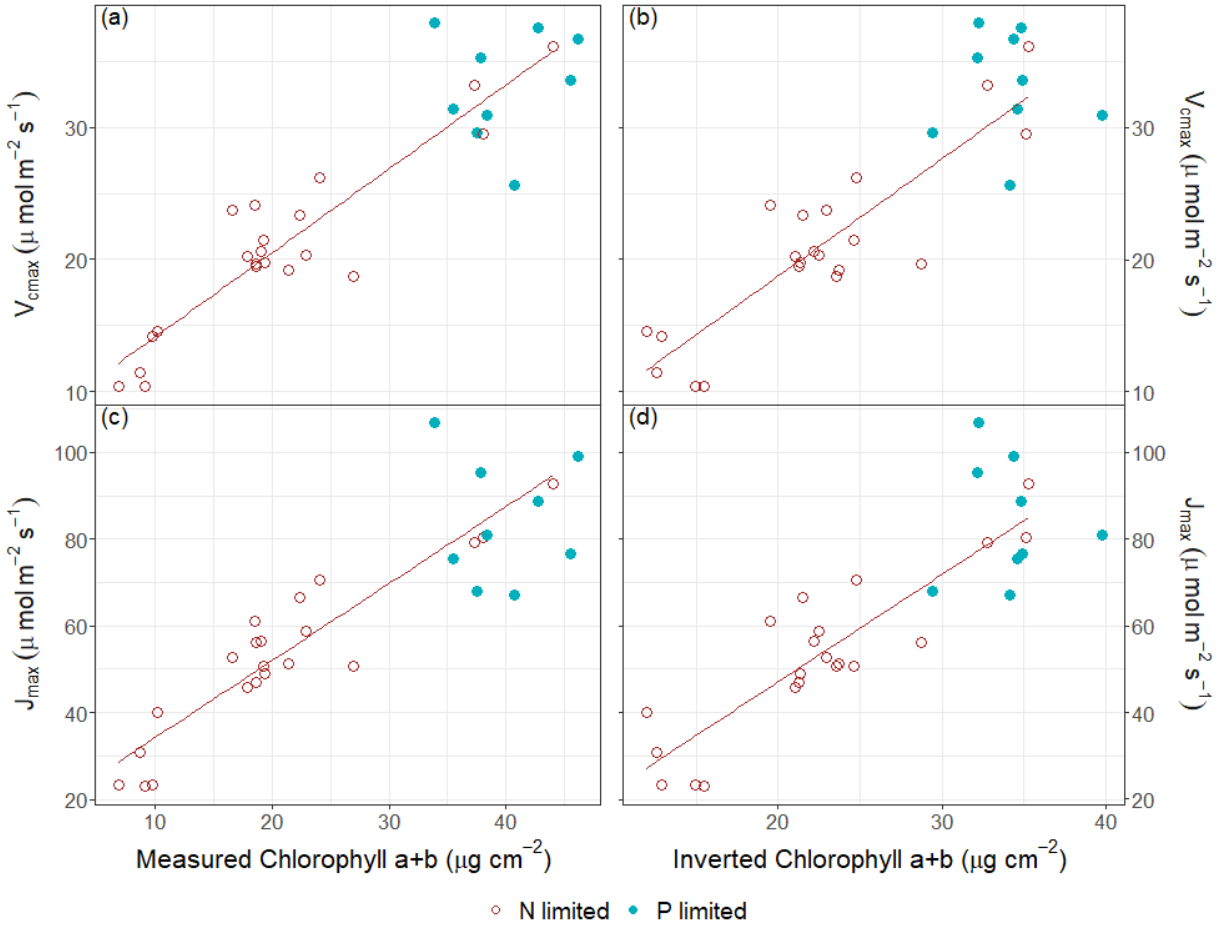

Figure 8. Relationships between measured chlorophyll$_{a+b}$ and inverted chlorophyll$_{a+b}$ and (a, b) V_{cmax} and (c, d) J_{max} under N (open brown circles) and P limiting conditions (filled teal circles). Lines have been fitted to relationships that are significant at P <0.05 with the brown lines fitted to N limited data.

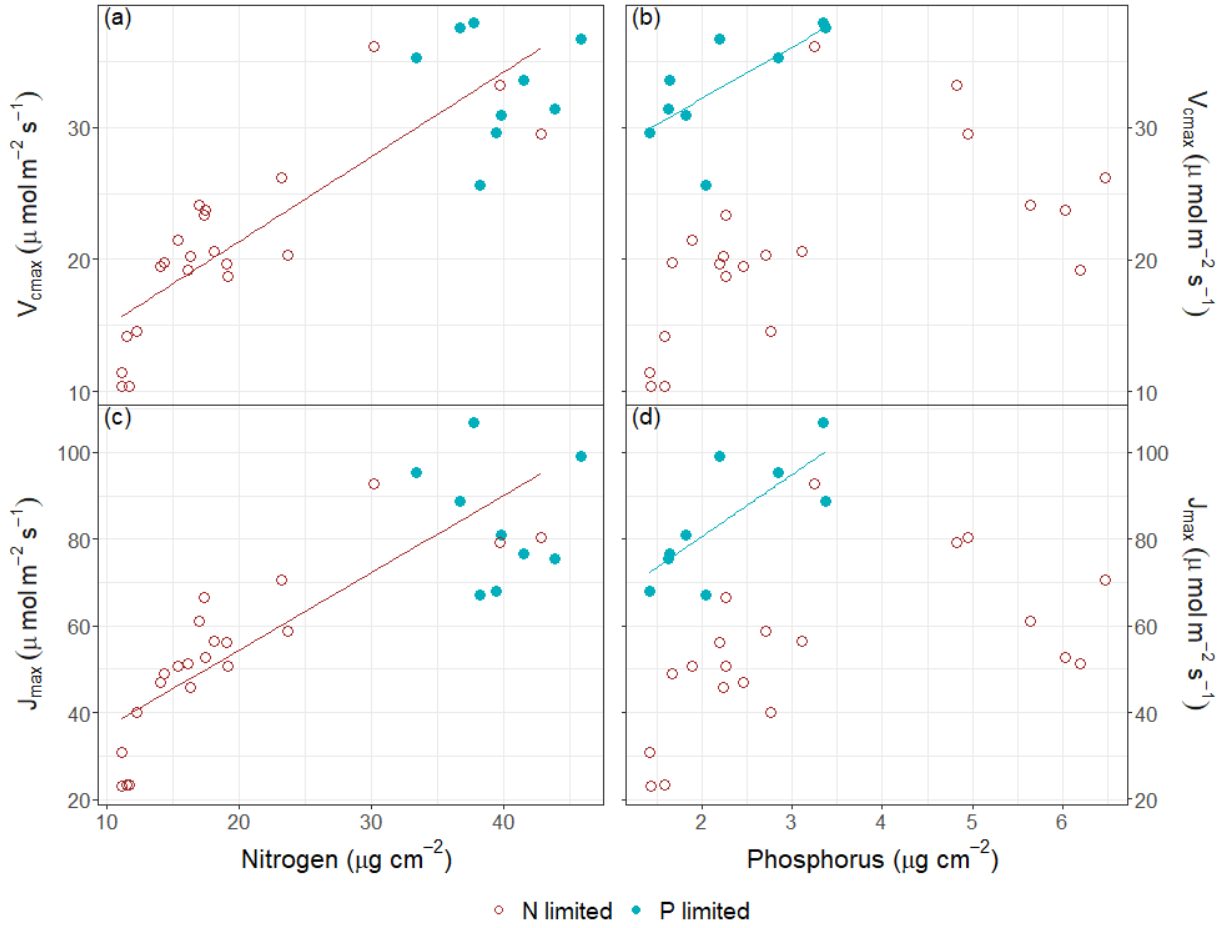

Figure 9. Relationships between area based nitrogen and phosphorus and (a, b) V_{cmax} and (c, d) J_{max} under N (open brown circles) and P limiting conditions (filled teal circles). Lines have been fitted to relationships that are significant at P <0.05 with the brown and teal lines fitted respectively to N and P limited data.

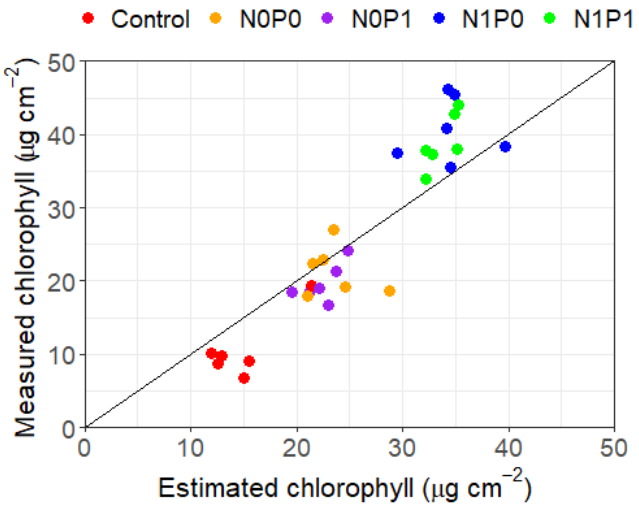

Figure 10. Relationship between measured chlorophyll and estimated chlorophyll derived from the PROSAIL inversion. The 1:1 line is shown as a solid line and treatments are denoted by filled circles with differing colours.

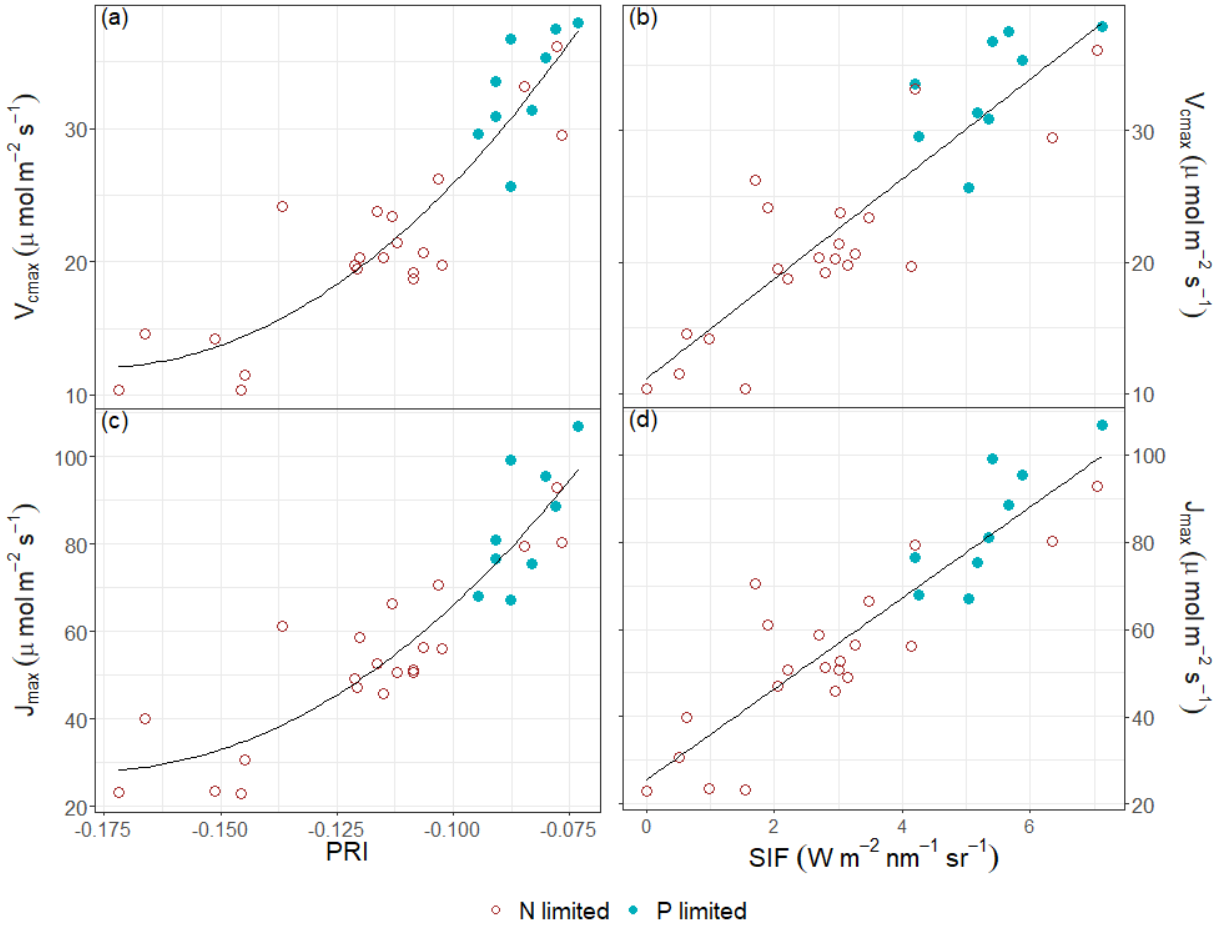

Figure 11. Relationships between Photochemical Reflectance Index and Sun Induced Chlorophyll Fluorescence and (a, b) V_{cmax} and (c, d) J_{max} under N (open brown circles) and P limiting conditions (filled teal circles). The black lines were fitted to the combined N and P limited dataset.

Appendix 1. Treatment variation in tree characteristics, photosynthetic variables, foliage nutrition, and predictor variables derived from hyperspectral data. Values shown include the mean followed by the standard deviation. Values presented for the ANOVA include the *F*-value followed by the *P* category, in which asterisks ***, **, represent significance at $P = 0.001$ and 0.01, respectively, ns = non-significant at $P = 0.05$. For all variables with significant treatment differences multiple range testing was undertaken using the Tukey test. Treatment values followed by the same letter were not significantly different at $P = 0.05$.

Variable	Control	N0P0	N0P1	N1P0	N1P1	ANOVA
Tree characteristics						
Height (cm)	54.2 (5.11)a	66.3 (7.07)a	63.2 (7.27)a	85.3 (19.8)b	85.8 (6.70)b	10.5***
Tree diam. (mm)	13.2 (1.88)a	12.9 (1.50)a	12.1 (1.45)a	14.7 (1.95)ab	15.9 (1.08)b	5.49**
Crown diam. (cm)	20.1 (3.70)a	22.4 (3.83)ab	19.2 (3.25)a	26.5 (3.33)bc	31.6 (2.36)c	14.3***
SLA (μg cm^{-2})	2,858 (573)	2,306 (518)	2,406 (226)	2,288 (234)	2,478 (647)	1.44^{ns}
Photosynthetic variables						
V_{cmax} (μmol m^{-2} s^{-1})	13.5 (3.60)a	20.6 (1.61)b	22.2 (2.87)b	31.3 (3.73)c	34.9 (3.16)c	46.6***
J_{max} (μmol m^{-2} s^{-1})	31.6 (10.8)a	54.7 (7.31)b	56.5 (8.36)b	77.9 (11.7)c	90.5 (10.3)c	32.3***
Foliage nutrition – mass based						
N (%)	0.447 (0.045)a	0.758 (0.120)b	0.759 (0.131)b	1.81 (0.127)c	1.58 (0.194)d	119***
P (%)	0.065 (0.019)a	0.093 (0.011)ab	0.214 (0.075)c	0.078 (0.013)ab	0.162 (0.039)c	15.7***
Chl_{a+b} (%)	0.399 (0.165)a	0.878 (0.140)b	0.849 (0.113)b	1.78 (0.192)c	1.68 (0.162)c	85.3***
Foliage nutrition – area based						
N (μg cm^{-2})	12.0 (1.21)a	18.4 (2.93)b	17.6 (3.05)b	41.4 (2.91)c	36.7 (4.50)c	105***
P (μg cm^{-2})	1.74 (0.51)a	2.26 (0.26)a	4.98 (1.74)b	1.79 (0.29)a	3.76 (0.89)b	14.3***
Chl_{a+b} (μg cm^{-2})	10.7 (4.42)a	21.4 (3.41)b	19.7 (2.63)b	40.6 (4.39)c	39.0 (3.76)c	71.2***
Derived predictor traits						
Inverted Chl_{ab} (μg cm^{-2})	14.9 (3.47)a	23.7 (2.82)b	22.4 (1.86)b	34.5 (3.27)c	33.7 (1.51)c	56.6***
PRI	-0.150 (0.018)a	-0.112 (0.006)b	-0.115 (0.012)b	-0.089 (0.004)c	-0.078 (0.004)c	42.4***
SIF (W m^{-2} nm^{-2} sr^{-1})	1.14 (1.11)a	3.08 (0.67)ab	2.46 (0.65)b	4.90 (0.54)c	6.04 (1.08)c	32.1***